Diagnostic fields developed for hourly updated NOAA weather models

Stanley G. Benjamin[1], Eric P. James[2,1], John M. Brown[1], Edward J. Szoke[3,1],
Jaymes S. Kenyon[3,2,1], Ravan Ahmadov[2,1], David D. Turner[1]

[1]NOAA Global Systems Laboratory
Boulder, CO
[2]Cooperative Institute for Research in Environmental Sciences, University of Colorado,
Boulder, CO
[3]Cooperative Institute for Research in the Atmosphere, Colorado State University,
Fort Collins, CO
[4]National Weather Service, Grand Rapids, MI (as of July 2021)

7 May 2020, updated 16 September 2021

Abstract

This document describes methods for diagnosing non-prognostic variables from explicit prognostic variables from hourly updated NOAA models. Many of these diagnostics have been developed for specific forecast applications for downstream forecast users over the years; these variables have been output from the **Rapid Update Cycle (RUC)** model prior to 2012, and from the **Rapid Refresh (RAP)** and **High-Resolution Rapid Refresh (HRRR)** models since 2012 and 2014, respectively. Some of these diagnostics are also being used for the **RTMA-3D** (experimental in 2021), as well. The code for these diagnostics resides within the Unified Post-Processor (Unipost or UPP) program, used for common NCEP modeling system output. This document serves as a reference for forecast users seeking to apply these model fields for their forecast applications.

Table of Contents

1. **Introduction**

   Table - History of hourly updated model (RUC/RAP/HRRR) versions

2. **Descriptions of diagnostics by category**

End of Table of Contents

1. Introduction

This document describes diagnostic output fields for the NOAA Rapid Refresh (RAP) and High-Resolution Rapid Refresh (HRRR) hourly updated weather models. These descriptions provide at least general information on the diagnostic techniques by which these fields are calculated but do not include code-level details. The diagnostic fields described in this document do not include *all* output fields from the RAP and HRRR but only those for which the diagnostic method was not obvious and description is needed for interpreting the fields by forecast users.

The RAP, with 13-km grid spacing, was implemented at NOAA/NCEP in 2012 after running experimentally at NOAA/ESRL Global Systems Division (GSD[1]) since 2009 (Benjamin et al. 2016). The HRRR, with 3-km grid spacing and explicit convection, was implemented at NCEP in 2014, but also ran experimentally at NOAA GSD since 2009 (Dowell et al. 2021; James et al. 2021). Many of the diagnostic techniques explained in this document were developed initially for use in the hourly updated Rapid Update Cycle (RUC, Benjamin et al. 2004) model run at NCEP from 1998-2012. Table 1 provides a history of the versions of the RUC, RAP, and HRRR models to clarify changes made to these diagnostics at certain points in code history.

Both the RAP and HRRR models use the common NCEP post-processing program, Unipost (also known as the Unified Post-Processor - UPP), which has been used for approximately the last decade for all NCEP models. The diagnostics described in this document are generated either in the UPP code or directly diagnosed within the WRF-ARW model used for RAP and HRRR. These diagnostic methods will be carried over for output fields from the new Rapid-Refresh Forecast System (RRFS) model, which is part of the Unified Forecast System that uses the FV3 dynamic core. The RRFS is currently under development and is planned to replace the HRRR model at NCEP in the 2023-2024 timeframe.

Graphical examples are shown in this memo for many diagnostic fields. All fields are stored in GRIB using SI (International System of Units) / metric units even though some graphics are displayed using conversion to non-SI units (e.g., knots, degrees Fahrenheit).

HRRR GRIB2 Tables:
Two-dimensional fields.
Native hybrid model level fields.
Isobaric level fields.
Sub-hourly fields.

RAP GRIB2 Tables:
Two-dimensional fields.
Native hybrid model level fields.
Isobaric level fields.

---

[1] The NOAA ESRL Global Systems Division (GSD) became the NOAA Global Systems Laboratory (GSL) in April 2020. We will use GSL and GSD interchangeably in this document.

Table 1. History of rapidly updated model and assimilation systems at NCEP (as of Feb 2021). Dates for implementation for experimental versions at NOAA ESRL/GSD/GSL are also shown. **RUC** = Rapid Update Cycle. **RAP** = Rapid Refresh. **HRRR** = High-Resolution Rapid Refresh. Experimental versions of the RAP and HRRR models are referred to in this document as RAPX and HRRRX, respectively.

Model and assimilation system	Horizontal grid spacing	Number of vertical levels	Assim. frequency	Implementation (month/year)		Geographical domain
				NCEP	**ESRL**	
RUC1	60 km	25	3h	**1994**		CONUS
RUC2	40 km	40	1h	**4/1998**		CONUS
RUC20	20 km	50	1h	**2/2002**		CONUS
RUC13	13 km	50	1h	**5/2005**		CONUS
RAP v1	13 km	51	1h	**5/2012**	**2010**	N. America
RAP v2	13 km	51	1h	**2/2014**	**1/2013**	N. America
RAP v3	13 km	51	1h	**8/2016**	**1/2015**	N. America
RAP v4	13km	51	1h	**7/2018**	**5/2017**	N. America
RAP v5	13km	51	1h	**12/2020**	**5/2019**	N. America
HRRR	3 km	51	1h	**9/2014**	**2010**	CONUS
HRRR v2	3 km	51	1h	**8/2016**	**4/2015**	CONUS
HRRR v3	3 km	51	1h	**7/2018**	**5/2017**	CONUS, Alaska
HRRR v4	3 km	51	1h	**12/2020**	**6/2019**	CONUS, Alaska

2. Descriptions of diagnostics by category

Diagnostic fields are grouped by variable type, each with a summary of the method. Significant changes between RAP/HRRR versions are noted along with the date of the change.

A. Humidity-related variables

i. Relative humidity

Relative humidity (RH) is always defined in the hourly updated models using _saturation with respect to wate_r at all levels regardless of air temperature in the RAP/HRRR isobaric fields and in the 2-m RH field. This approach is consistent with the RH approach used for NAM but not for GFS as of April 2012. Examples are shown for 850-hPa RH, and 850-500h-Pa mean relative humidity graphics (see Figs. 1-2).
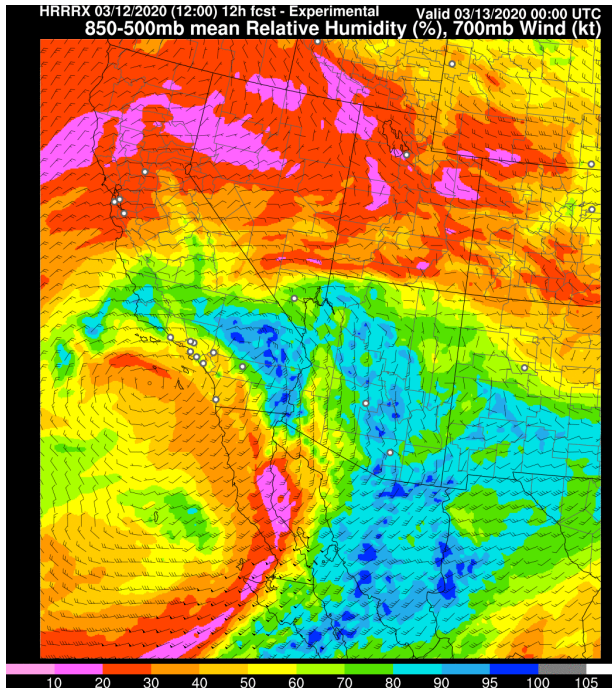

Fig. 1: 850-hPa RH. From 12-h HRRRX forecast valid at 00 UTC 13 Mar 2020. The RH fields show deep moisture surging northward into the southwestern CONUS associated with an approaching upper-level low.
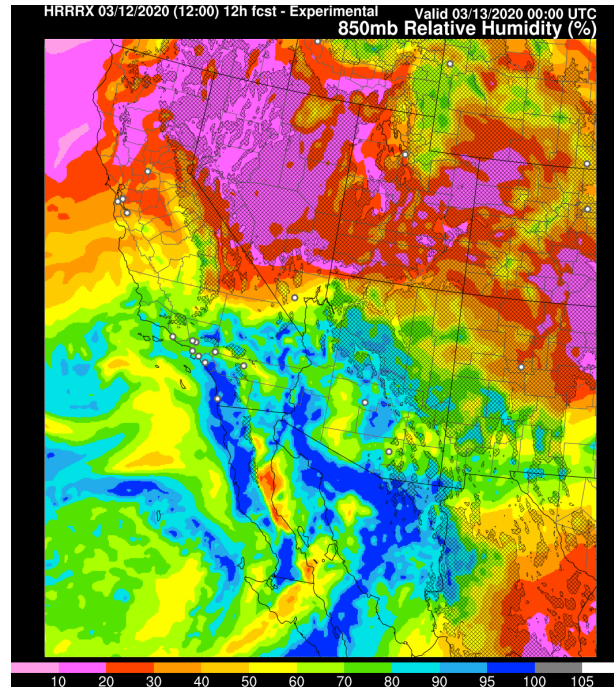
Fig. 2: Mean RH for 850-500-hPa layer. From 12-h HRRRX forecast valid at 00 UTC 13 Mar 2020. Note that regions where the ground is at a lower pressure than 850 hPa are shown as hatched.

ii. Precipitable water

Precipitable water (PW), which is the vertically integrated water vapor in a column (Fig. 3), is defined in a manner consistent with meteorological convention, where water-vapor specific humidity at each vertical level is multiplied by the vertical pressure thickness of that level, and then summed over the model atmosphere to the model top (10 hPa for RAP, 15 hPa for HRRR). This diagnosed PW is relative to the model surface elevation at a given gridpoint, so this field will usually show topographically-related variations as in the example below over ridges in the state of Nevada and also over the Sierra Nevada mountains in California and into Baja California (Mexico).
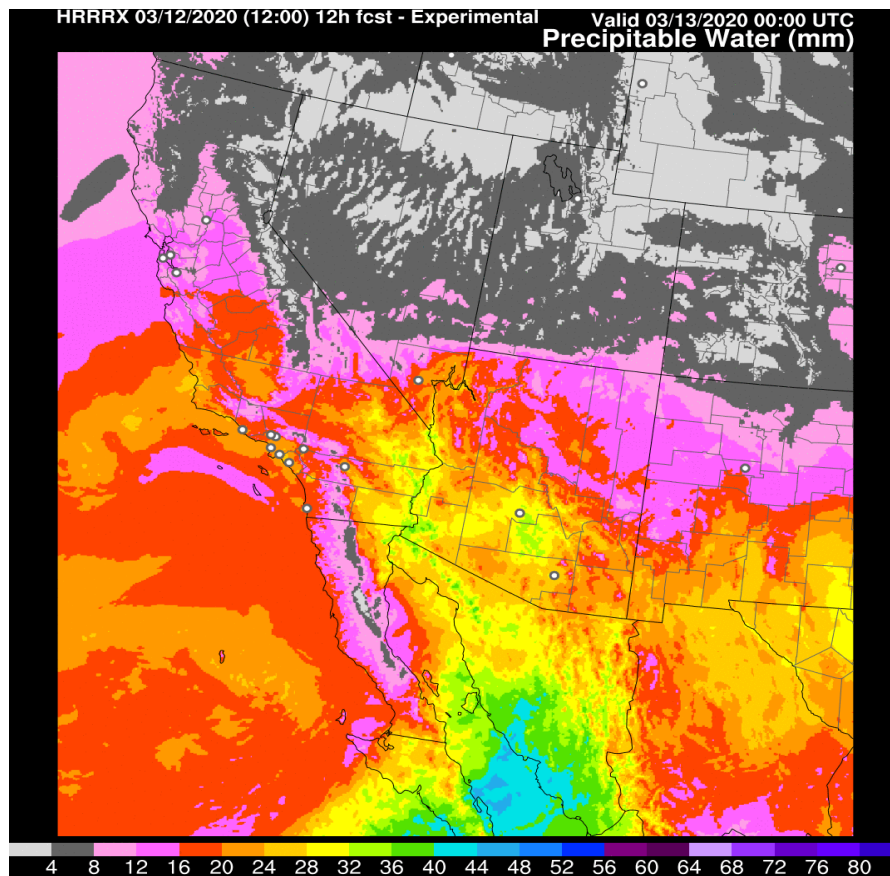

Fig. 3: Precipitable water. From 12-h HRRRX forecast valid at 00 UTC 13 Mar 2020. (Another example of using a table)

iii. Relative humidity with respect to precipitable water

A total-column RH with respect to precipitable water (RHPW) is defined as the ratio between precipitable water (PW) and PW if the full column was completely saturated with respect to water, i.e., **RHPW = PW / PW(sat)**. Figure 4 shows an example of RHPW. RHPW provides more continuity, especially across terrain variations, than PW (compare Fig. 4 below with Fig. 3 above). It is a relative-humidity measure through *all* levels, more so than the 850-500 hPa RH product. RHPW shows similar patterns to 850-500 hPa RH. The 850-500 hPa RH gives a linear average of RH over pressure intervals. RHPW is weighted more heavily toward layers with warmer temperatures with much higher saturation vapor pressure; i.e., a 'Clausius-Clapeyron-weighted' measure of vertically integrated RH.

Fig. 4: Relative humidity with respect to precipitable water (RHPW). From 12-h HRRRX forecast valid at 00 UTC 13 Mar 2020.
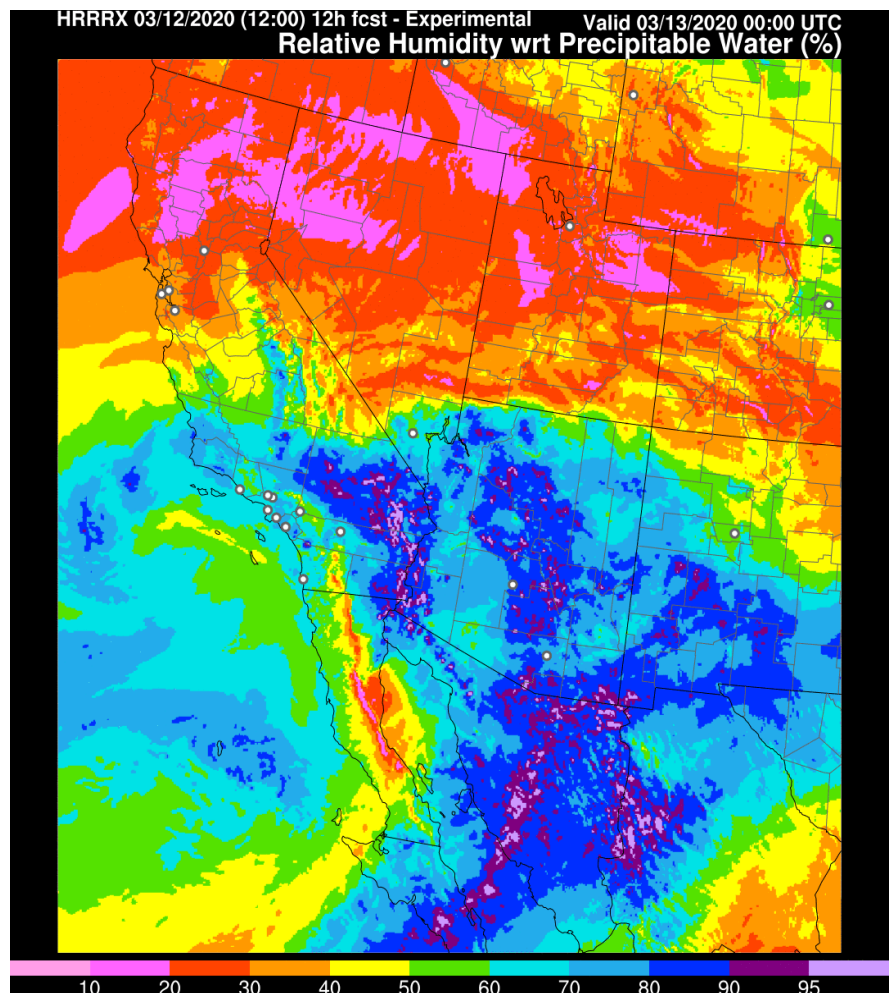
B. Surface and boundary-layer variables

i. 2-m temperature

The 2-m temperature (Fig. 5) is diagnosed internally in the model in a surface-diagnostics subroutine in the RAP/HRRR configuration of the WRF-ARW model using atmospheric temperature, skin temperature, and fluxes on the lowest prognostic model level.   This field is diagnosed because the lowest model level in sigma coordinates is currently 0.999-sigma or ~8 m above ground level (AGL). Analyzed 2m temps for RAP/HRRR use the analysis increment at the lowest model level added to the background 2-m temp value. (Note: the 2-m temperature and dewpoint temperatures in RAP or HRRR do not use a more detailed "minimum topography" field as in the RUC - Benjamin et al. 2004, p.507.)

The 2m temperature is valid at the *model* terrain elevation at the same grid point. Therefore, estimates for 2m temperature at the same horizontal point but using a different elevation should be estimated using local lapse rate information as described in Benjamin et al. (2004, section 3.c).
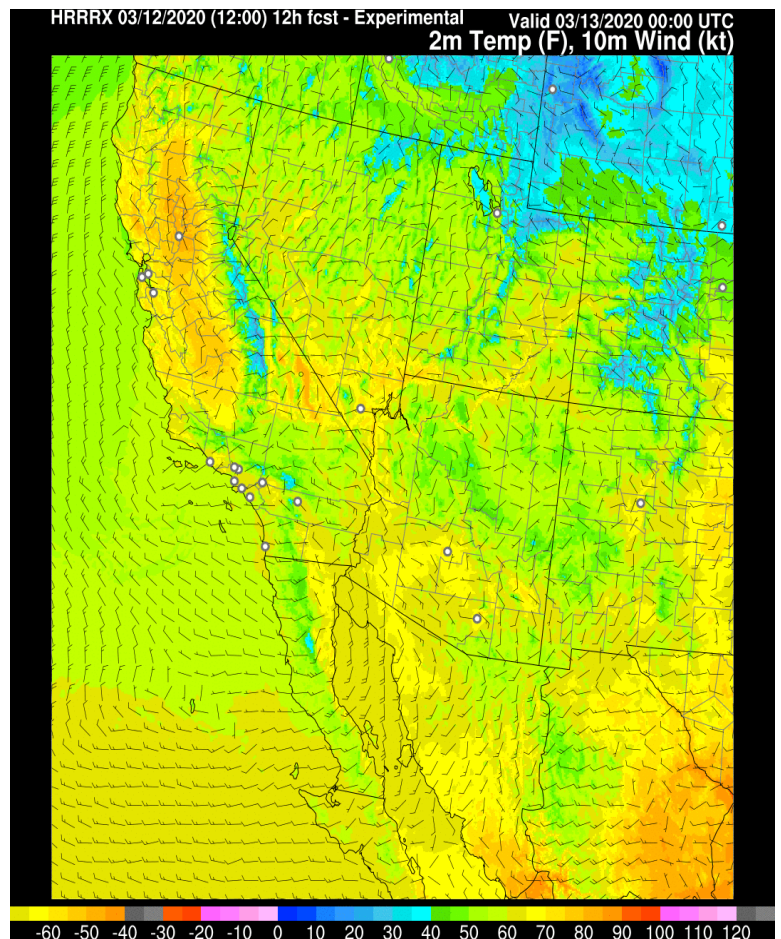

Fig. 5. 2-m temperature.

ii. 2-m dewpoint

The 2-m dewpoint temperature (Fig. 6) is calculated directly from temperature, specific humidity, and pressure at the lowest prognostic model level (currently 0.999-sigma or ~8 m AGL).
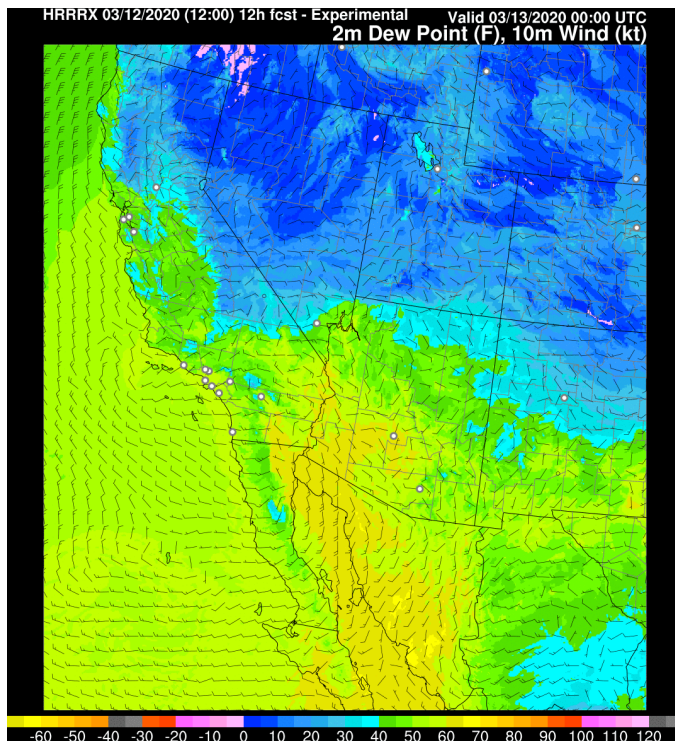

Fig. 6. 2-m dewpoint temperature. The HRRR website displays 2-m dew point (in °F) combined with a wind barb display of 10-m wind (in knots, long barb = 10 knots, half barb = 5 knots). Shown here are 12-h forecasts valid 00z/13 Mar 2020 from the 12z/12 Mar HRRRX.

iii. 10-m wind

Prior to RAPv4/HRRRv3 (2018), the 10-m wind was calculated directly from the lowest prognostic model level (currently 0.999-sigma, about 8 m AGL at sea-level, slightly less for higher elevations). Starting in 2018 (RAPv4, HRRRv3), this lowest model level wind is interpolated to 10 m AGL. This 10-m wind estimate is made within the WRF model itself (in the MYNN surface layer routine) using native level data from the model at the k=1 and k=2 levels and interpolating between these levels.

An hourly maximum 10-m wind is also diagnosed from values at each model time step for each horizontal grid point.

iv. 80-m wind speed

The 80-m wind speed is estimated internally within the WRF model by interpolation between the appropriate prognostic model levels. Wind speed at this level has been useful as a nominal hub-height wind speed for wind energy applications, but it is also useful as another metric for wind gust potential.

v. PBL depth

For RAPv2/HRRRv1 and prior models, the PBL depth (or height) was diagnosed using the vertical profile of virtual potential temperature (θ_v) from the model native levels. The algorithm searched for the height above the surface at which θ_v again exceeds θ_v at surface (lowest native level - 8 m above surface). The surface θ_v is boosted by an additional 0.5 K, which does not strongly affect the PBL height if it is already at least 100 m, but does avoid a diagnosis of zero depth from a small (< 0.5 K) inversion in the lowest 20 m. Units: Distance above surface in meters.
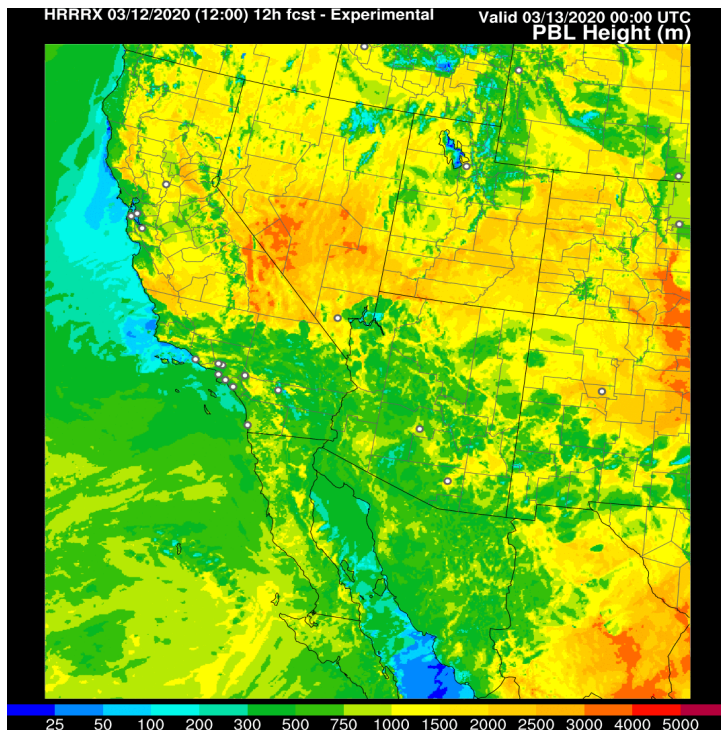
For RAPv3/HRRRv2 and subsequent models, the PBL height is now diagnosed directly in the model MYNN PBL scheme (Olson et al. 2019a,b) using a hybrid PBL diagnostic based on turbulent kinetic energy when the sensible heat flux is low (stable conditions) and the θ_v profile (as used before) when sensible heat flux is larger. An example is shown in Fig. 7. **Note**: A separate PBL depth using only the θ_v profile continues to be used for diagnosing *gust wind speed potential*.

Fig. 7. Planetary boundary layer (PBL) height (m). From the 12-h HRRRX forecast valid at 00 UTC 13 Mar 2020.

vi. Gust wind speed potential

The gust wind speed potential diagnostic is for the *potential* for wind gusts, and will often exceed the observations of transient wind gusts at a particular time. It is very dependent on the PBL depth diagnostic. The diagnostic calculates the excess of wind speed over surface speed at each level below the PBL depth. This excess is then multiplied by a coefficient **(f(z))** that decreases with height from 1.0 at the surface to 0.5 at 1 km height AGL, and is 0.5 for any height > 1 km AGL. The maximum weighted wind excess is then added back to the surface wind [i.e., **gust-potential = vsfc + max (f(z)*(v(k)-vsfc)**]. This calculation is roughly illustrated by the graphic below.
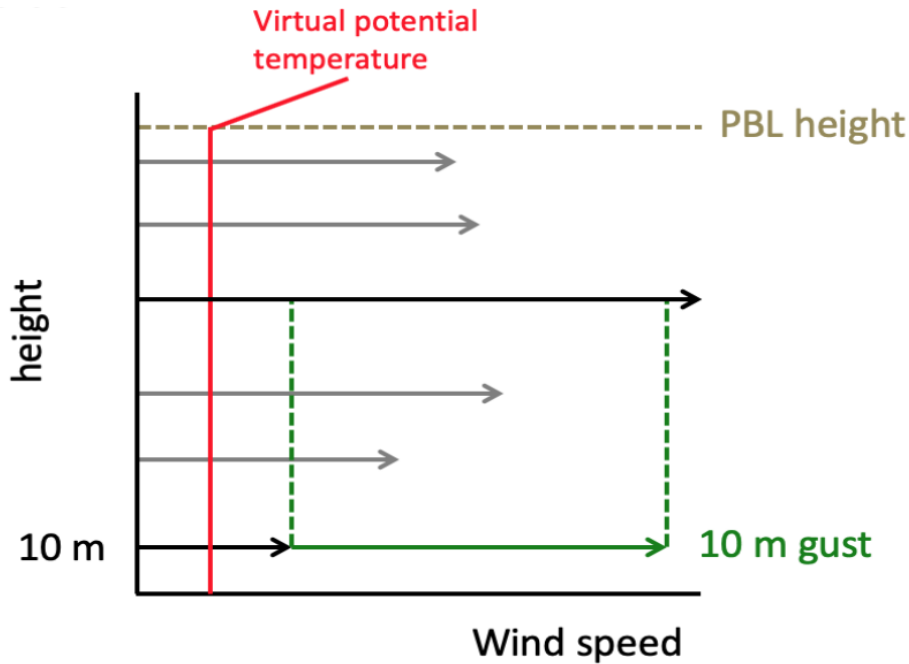
Horizontal axis is for both wind speed and also for virtual potential temperature (in red).

Note that the gust wind speed potential was temporarily larger at night in RAPv3/HRRRv2 due to the hybrid PBL depth diagnostic. On 13 Oct 2016, the ESRL/GSD experimental RAPv3/HRRRv2 changed back to using the θ_v-profile-based PBL depth diagnostic for wind gust speed potential calculation. The NCEP operational RAPv3/HRRRv2 made this same change on 2 Nov 2016. Wind fields from a HRRR forecast, including the gust speed potential diagnostic, are shown in Fig. 8.
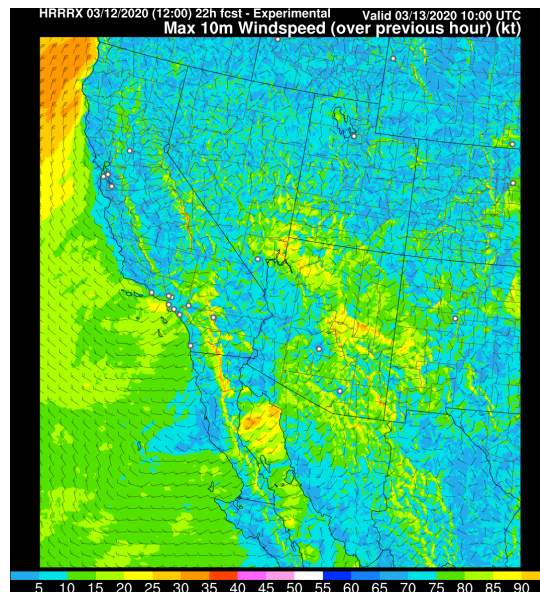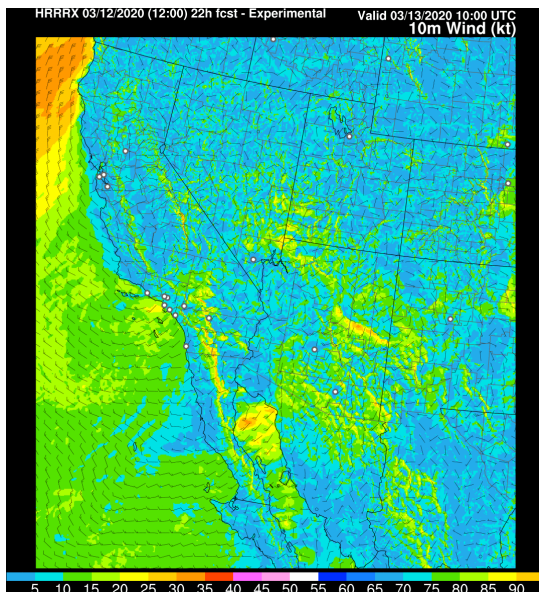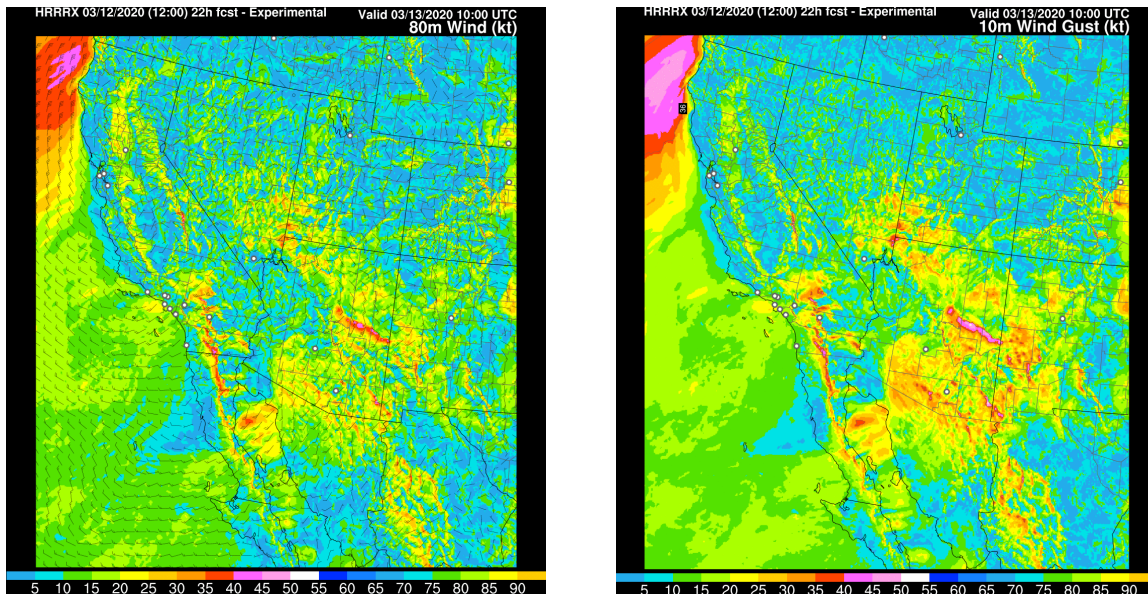
Fig. 8. Near-surface wind fields for 22-h HRRRX forecasts (kts) valid at 10 UTC 13 Mar 2020. This is the approximate time of the strongest wind downstream of the Mogollon Rim in Arizona following passage of an upper-level trough axis. Panels show (top left) 10-m winds, (top right) maximum 10-m wind over previous hour, (bottom left) 80-m winds, and (bottom right) **10-m wind gust speed potential.** There are instances when the 80-m wind may give the best forecast of the maximum 10-m wind gust potential.

C. Surface-pressure-related variables

i. Sea-level pressure

The RAP and HRRR use the MAPS reduction ([Benjamin and Miller 1990](#)) to calculate sea-level pressure. This reduction uses the 700-hPa temperature to minimize unrepresentative local variations caused by local surface temperature variations (used in most other reduction methods). This method improves over the standard reduction method in mountainous areas and gives geostrophic winds that are more consistent with observed surface winds (Fig. 9).

Fig. 9. MAPS sea-level pressure diagnostic. MSLP is displayed as a contoured field (every 2 hPa) with the 1-h total precipitation field as a graphic (in inches). Shown here are 12-h forecasts valid 00z/13 Mar 2020 from the 12z/12 Mar HRRRX.
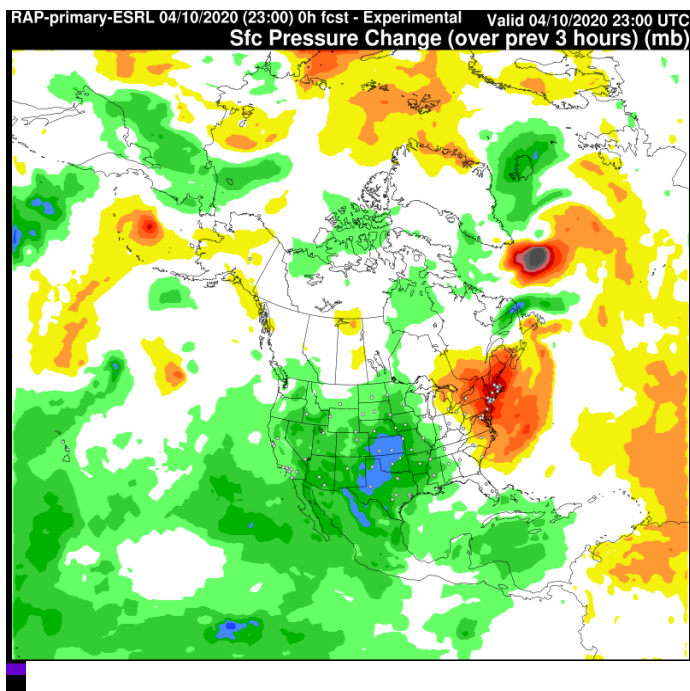
13
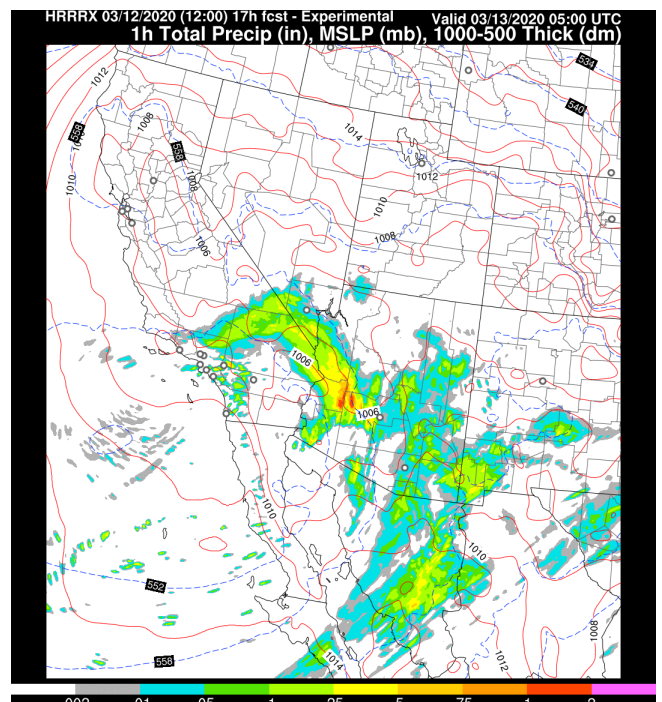
ii. 3-h pressure change

Fig. 10. 3h surface-pressure change. From RAPX analysis valid 2300 UTC 10 April 2020.

This field is determined in NOAA/GSL website plots (for RAP and HRRR models) by differencing surface pressure fields at valid times separated by 3 h (Fig. 10). The output file variable is surface pressure itself, but no surface pressure change is output (in GRIB) since it can be calculated separately.

This field is available for analysis times and forecast times. For the analysis times, observed altimeter setting values (converted to surface pressure) are used in the RAP/HRRR analyses, so this change field reflects the observed 3-h pressure change fairly closely over areas with surface observations. Analyzed surface pressure can also change from the 3-d data assimilation using non-surface observations, so 3-h pressure change between analyses also roughly reflects actual change over the full domain but less precisely in areas without surface observations.

The 3-h pressure change field during the first 3 h of a model forecast often shows some non-physical features resulting from gravity wave sloshing in the model, despite use of digital filter initialization (DFI) in the RAP/WRF model (Peckham et al. 2016). The smaller-scale features in this field appear to be very useful for seeing predicted movement of lows, surges, etc. despite some slosh at the beginning of the forecast.

D. Soil-land-lake-related variables

i. Soil temperature and moisture

Soil moisture at different levels is cycled continuously in the RAP/HRRR model/assimilation cycles without resetting from external models. There are 9 levels in the RUC land-surface model (Smirnova et al 2016) used in the RAP/HRRR configurations of WRF, extending down to 3 m deep. Soil moisture fraction is calculated as the soil volumetric moisture divided by the full volume of the soil. The *surface* soil moisture (fraction) is for the top 0.5 cm of soil only, so this field responds quickly to recent precipitation or surface drying. In general, the deeper in the soil, the more slowly do soil conditions change. The maximum soil moisture fraction is dependent on the soil-type-dependent value of porosity. Fig. 11 shows soil moisture fraction at the surface, and at 30cm depth, while Fig. 12 shows soil moisture availability (in percent). Soil temperature (Fig. 13) is defined at the same 9 levels in the RUC land-surface model.
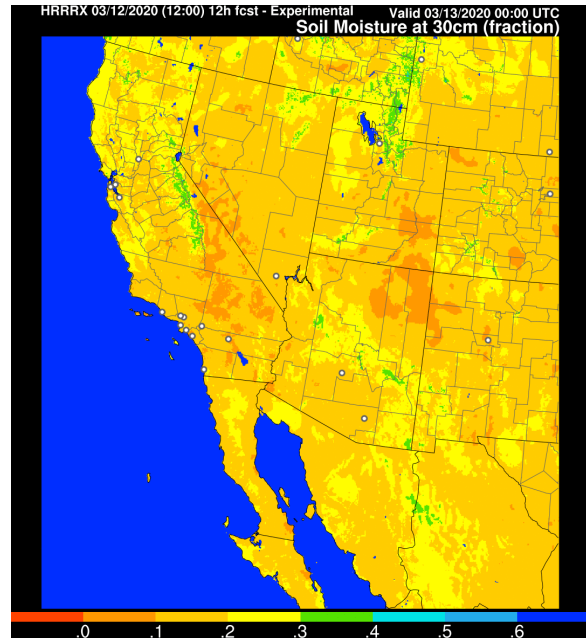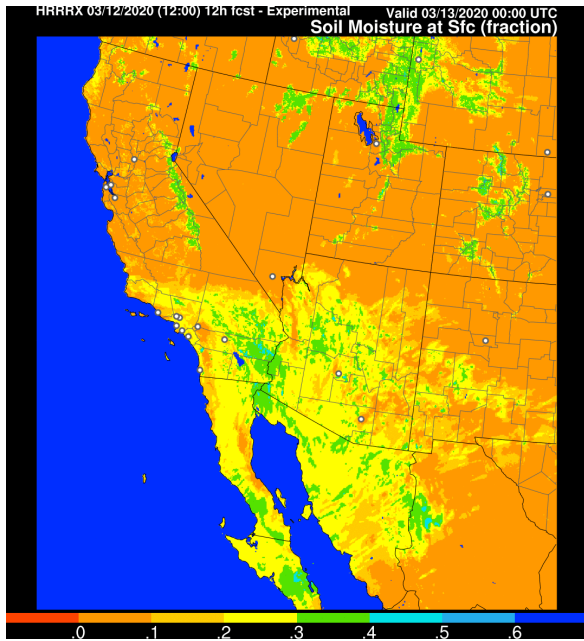
Fig. 11. Soil moisture fraction. 12-h Experimental HRRR forecasts from the 12z/12 Mar 2020 run valid at 00z/13 Mar for two of the 9 levels of moisture in the land-surface model, the surface (0.5 cm) on the left and for a depth of 30 cm on the right. Fraction (of total possible moisture).
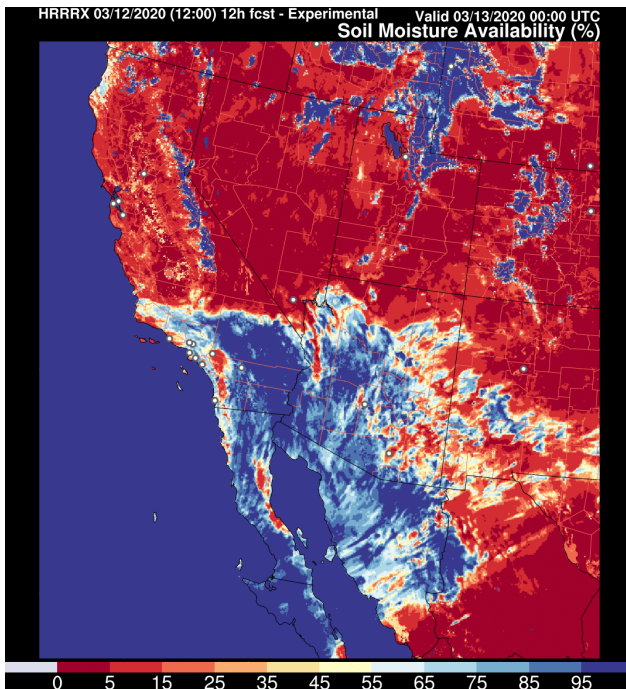

Fig. 12. Soil moisture availability. Units - percent, calculated in the top 0.5 cm layer. This is again a 12-h forecast valid 00z/13 Mar 2020 from the 12z/12 Mar HRRRX.
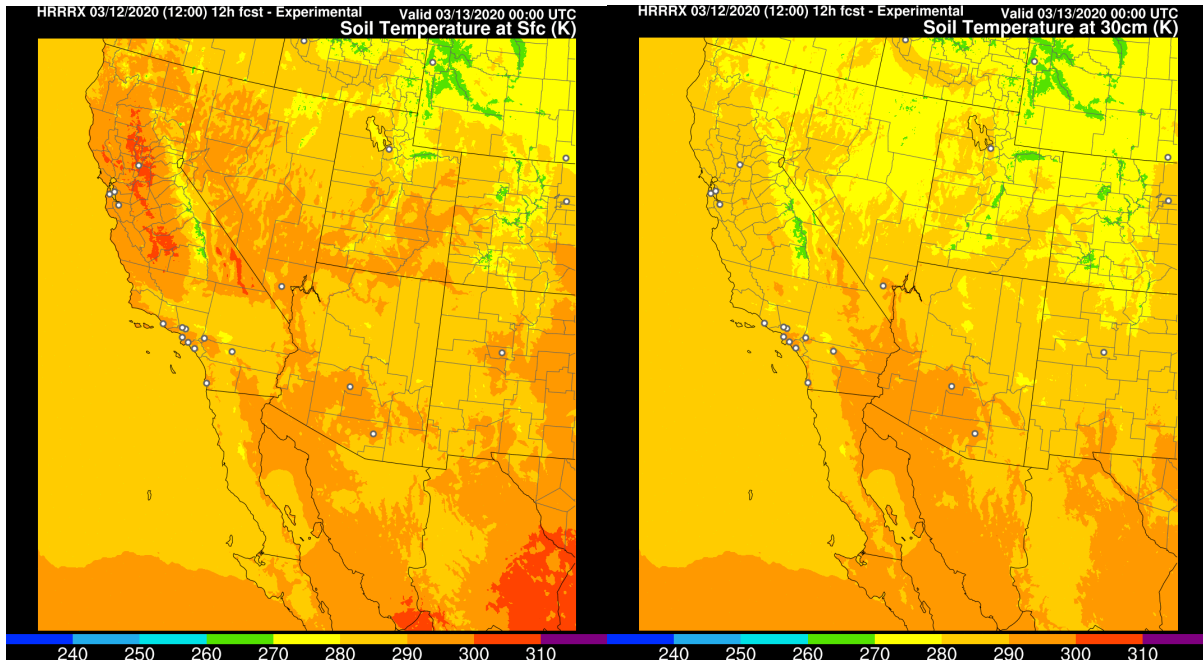
Fig. 13. Soil temperature (K) for surface (top 0.5 cm -left) and 30-cm level (right). From 12-h HRRRX forecasts from the 12z/12 Mar 2020 run valid at 00z/13 Mar.

ii. Skin temperature

Skin temperature (Fig. 14) is the temperature of the top level (1-cm depth) in the 9-level soil model (Smirnova et al 2016) over land, and the sea-surface (or lake-surface) temperature over water. Skin temperature will also be from the top snow level in the 2-layer snow model for grid points with snow cover. Skin temperature will vary in time for soil and snow-covered grid points, and starting with HRRRv4, also for small lakes.

Fig. 14. Skin temperature. From 12-h forecast valid 00z/13 Mar 2020 from the 12z/12 Mar HRRRX. Graphic in ºF.

E. Precipitation variables

i. Precipitation

All precipitation values in the RAP and HRRR, for all accumulation intervals including the model run total, are *liquid equivalents*, regardless of whether the precipitation is rain, snow, or other frozen precipitation. (In one e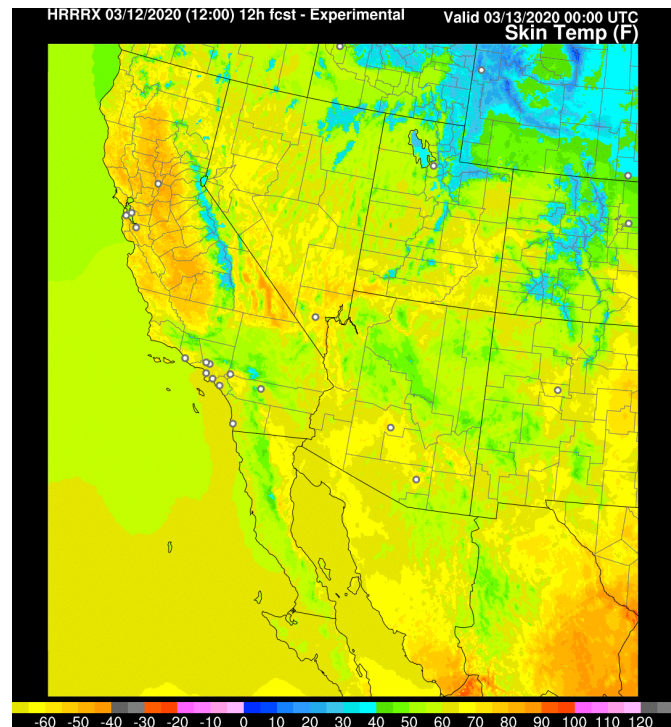xception, snow accumulation products are available both for liquid equivalent and in snow depth using temperature-dependent variable density instead of a simple 10-1 snow/water ratio). The run-total accumulated precipitation is the precipitation accumulated since the model initialization time. The 1h precipitation is the precipitation accumulated over the previous hour. The 15-minute precipitation (available in HRRRv4/2020) is the precipitation accumulated over the previous 15 minutes. Note that the RAP and HRRR do not output 3-h or 6-h precipitation, although these can be calculated by differencing the appropriate output files. The instantaneous precipitation rate is the total precipitation (resolved and sub-grid-scale) from the last physics time step and is written in mm/s.

Note that the RAP uses a convective parameterization scheme to represent sub-grid scale (finer than 13-km grid spacing) precipitation. Prior to 2015, the RAP used the Grell-Dévényi (2002) convective parameterization and has been using the Grell-Freitas scheme (Grell and Freitas 2014, ACPD) since 2015. As in most other convective parameterization schemes used at similar horizontal grid spacings, this scheme is not designed to completely eliminate grid-scale saturation in its feedback to temperature and moisture fields. One result of this is that the precipitation from weather systems that might be considered largely convective will nevertheless be reflected in the RAP model with a substantial proportion of resolvable-scale precipitation. Thus, the sub-grid scale precipitation from RAP should not be considered equivalent to "convective precipitation".
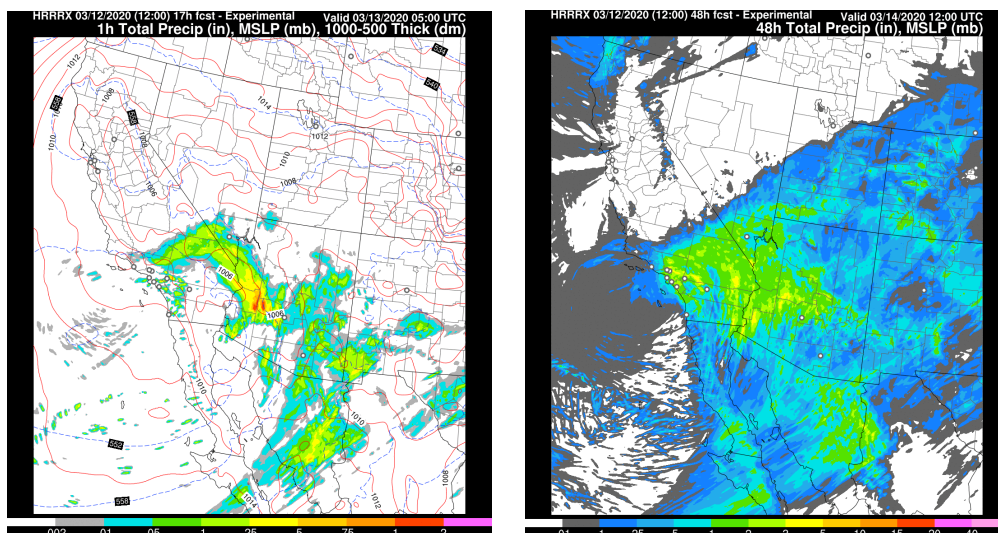
The various precipitation fields available on the GSL HRRR/RAP websites are shown below (Figs. 15-17).

Fig. 15. Basic precipitation fields: 1-h precipitation and MSLP (left) and run-total precipitation (right), in inches. For forecast initialized at 12 UTC 12 March 2020.
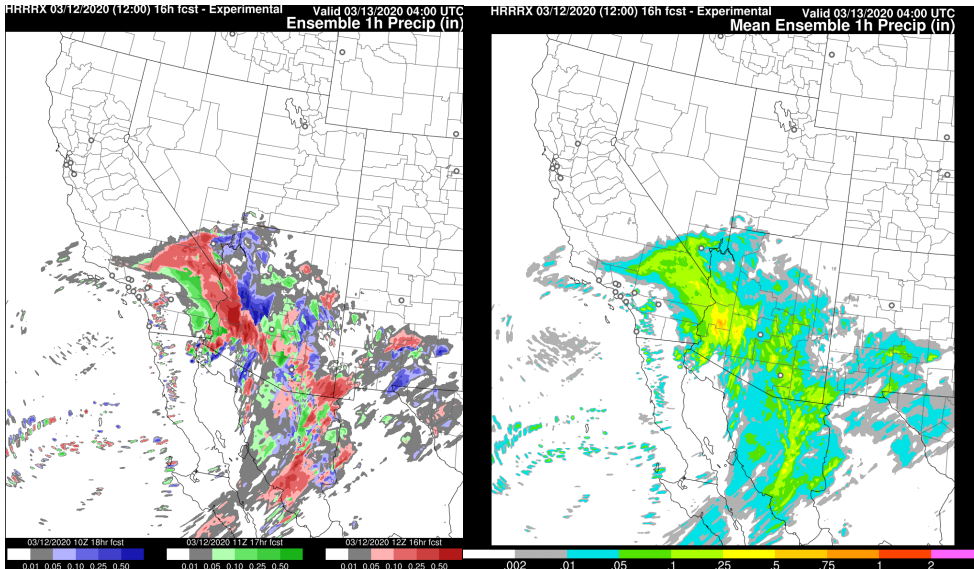
Fig. 16. Time-lagged ensemble 1-h precipitation fields valid for the hour ending at 04z/13 Mar. On the left is the 1-h precipitation from three HRRRX runs valid at 04z: the 16-h forecast from the 12z run, 17-h forecast from the 11z run and 18-h forecast from the 10z run. On right, the mean of these 3 runs is displayed. Note that the 16-h forecast is the last one where all three time-lagged members would be available since the current HRRR, for all run times, goes out to at least 18 h.

Fig. 17. Time-lagged for run-total model forecasts *(current, 1h previous, 2h previous) ensemble forecasts. similar to Fig. 16. except for* <u>*total*</u> *precipitation.*

ii. Snow/sleet accumulation

Two products are available for snow accumulation using **fixed** or **variable density**. For NCEP RAP/HRRR forecasts until summer 2015, snow and sleet were combined into a single product called "snow accumulation." This **fixed-density snow accumulation** is calculated using a **10:1 snow-water ratio** from the accumulated sno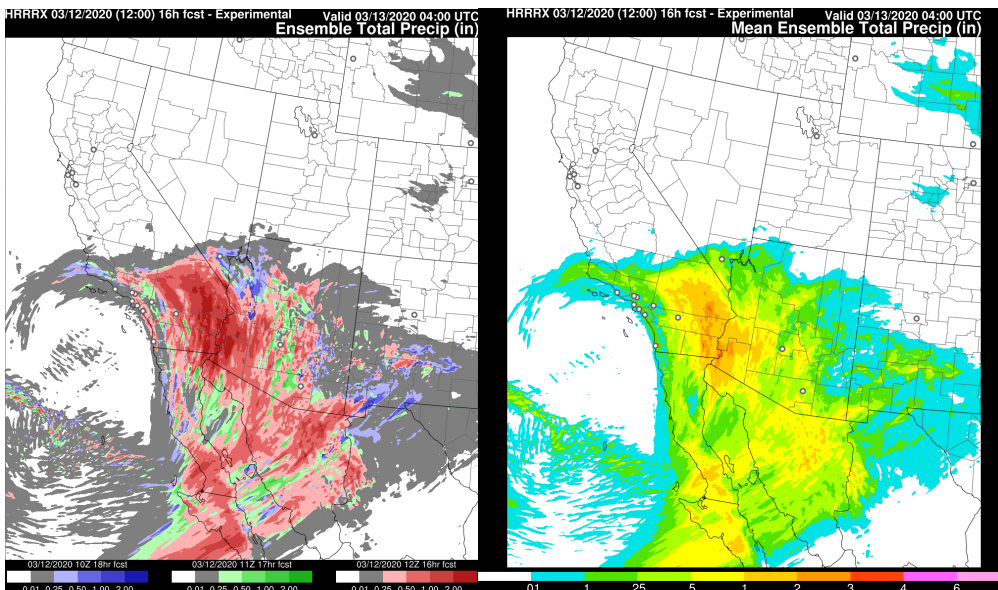w water equivalent with both snow and graupel/sleet combined. This ratio varies in reality, but the ratio used for this product was set at this constant value so that users will know the water equivalent exactly. The snow accumulation (through the snow liquid water equivalent) is explicitly forecast through the mixed-phase cloud microphysics in the model and specifically from snow mixing ratio and graupel mixing ratio fall out to the surface. The graupel field means that this snow/sleet accumulation field includes both sleet and even graupel from convective storms, especially in the 3-km HRRR model. This addition of sleet/graupel into snow accumulation was ended for RAP/HRRR runs by ESRL as of 3/3/2015 and was ended at NCEP with the RAPv3/HRRRv2 implementation in Aug 2016.

Starting 3/3/2015, snow accumulation in ESRL experimental versions of RAP and HRRR now use only actual snow accumulation and no longer use graupel/sleet accumulation. This change was propagated to the NCEP versions of RAP and HRRR (RAPv3/HRRRv2) in Aug 2016. The Thompson (Thompson 2008, Thompson and Eidhammer 2014) microphysics used in RAP and HRRR calculates explicitly the fall of snow mixing ratio (qs), graupel mixing ratio (qg), and rain mixing ratio (qr) reaching the surface, using separate fall speeds for each. This allows separate diagnosis of accumulation for each variable.

Since late 2015, *variable density* **snow accumulation** is also provided from the experimental RAP and HRRR (added to operational RAPv4/HRRRv3 2018). This accumulation variable uses variable snow density, which can vary using a snow-water ratio (inverse density) from less than 5:1 up to 17:1. The accumulation uses both snow and graupel (sleet) and even includes a subtraction from melting of fresh snow to obtain an estimate of what might be measured with a stick on a snowboard (see Fig. 18).
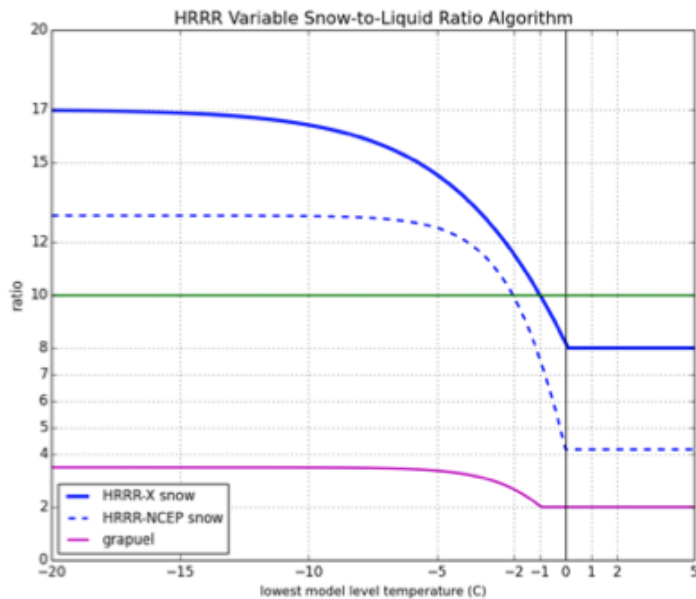
Fig. 18. Snow density as a function of near-surface air temperature each time step for **variable snow accumulation** product. In this figure, 'HRRR-NCEP' designates HRRRv3/RAPv4, and 'HRRRX' designates HRRRv4/RAPv5.

iii. Graupel accumulation

Graupel accumulation (Fig. 19) is defined as the model-internal accumulation at the surface, timestep-by-timestep, of graupel (qg) as defined by Thompson (2008) and Thompson and Eidhammer (2014). This graupel can occur from either winter-storm sleet or convective-storm ice/ graupel formation.

Fig. 19. Graupel accumulation. 48-h total accumulation of graupel ending at 12z/14 March from the 12z/12 March 2020 HRRRX.
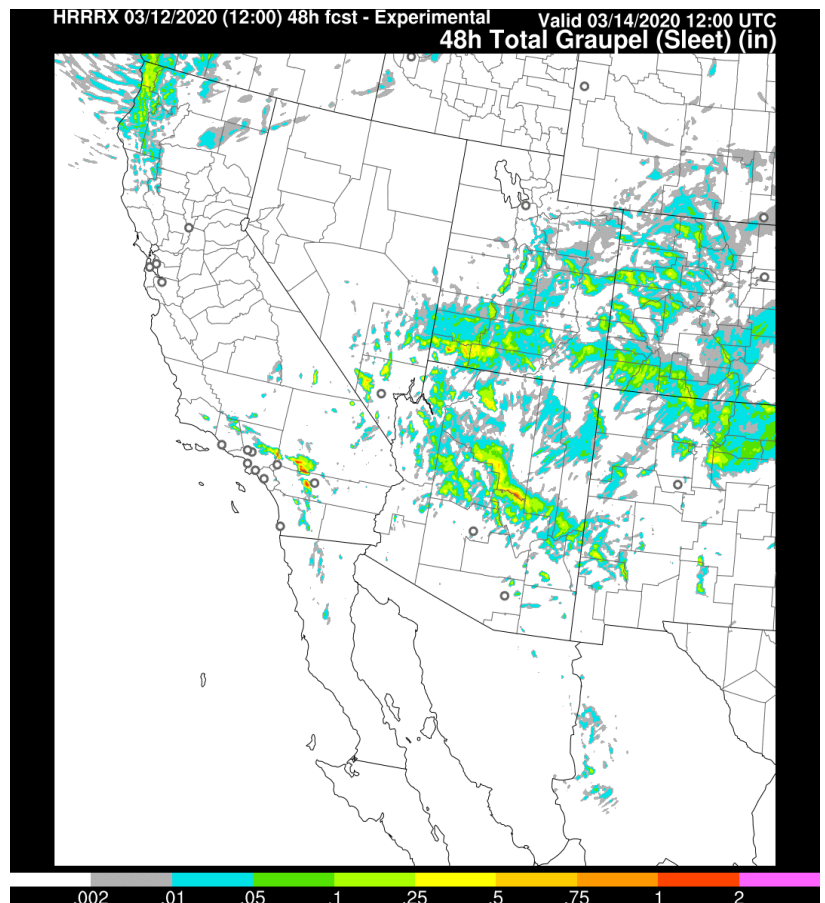
iv. Freezing rain accumulation

The freezing rain accumulation (Fig. 20) is calculated by accumulating a special class of rainfall, timestep-by- timestep, but only including values when the temperature at the lowest level < 0 ℃ at that specific timestep.

Fig. 20. Freezing rain accumulation. For 48-h total forecast accumulation ending at 12z/14 March from the 12z/12 March 2020 HRRRX.
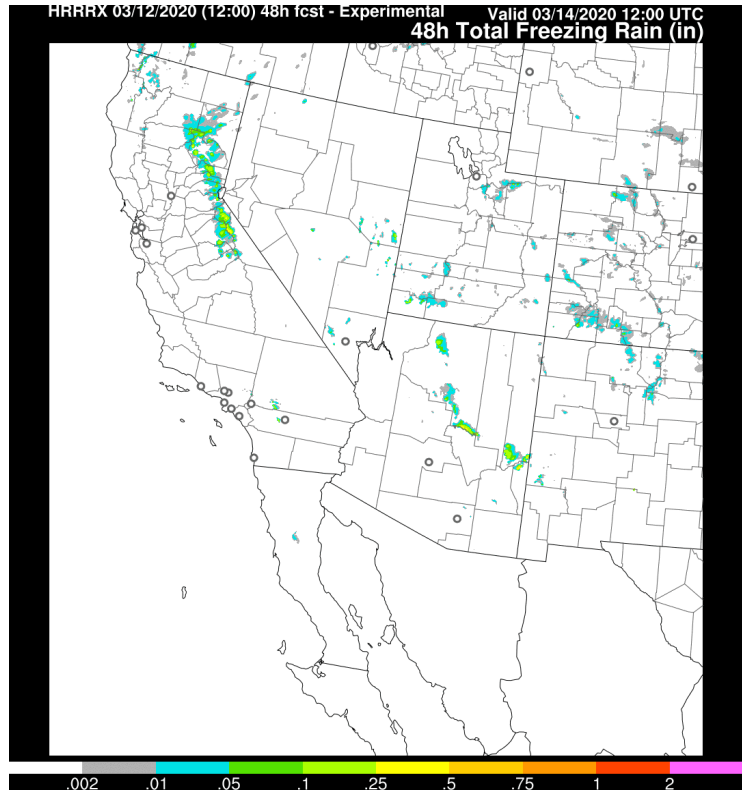
v. Frozen precipitation percentage

This field (Fig. 21) uses the explicit precipitation (rain, snow or graupel) produced from the multi-species Thompson cloud microphysics scheme. It is calculated as (snow-accumulated + graupel-accumulated) divided by (snow-accumulated + graupel-accumulated + rain-accumulated). No rime factor (as used on the Ferrier microphysics scheme - Aligo et al. 2018) is used in this explicit calculation.

Fig. 21. Frozen precipitation percentage. For 17-h forecast valid for the previous 1-h period valid at 05z/13 March from the 12z/12 Mar 2020 HRRRX.
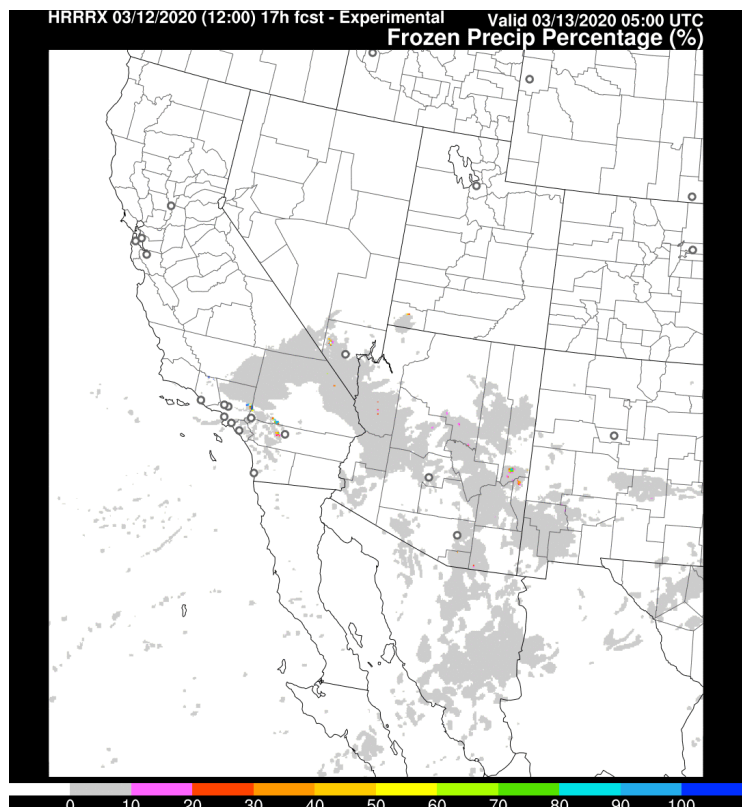
vi. Snow depth

This field is the current estimated snow depth on the surface using the latest snow density, which is also an evolving variable (snow-water equivalent cycles internally within the RAP or HRRR 1h cycle). The 10:1 ratio is kept only for fresh snow falling on the ground surface when 2-m air temperature is below -15 °C. When 2-m temperature is above -15 °C the density of falling snow is computed using an exponential dependency on 2-m temperature, and usually the ratio will be less than 10:1, but not less than 2.5:1. The density of snowpack is computed as the weighted average of old and fresh snow, and it changes with time due to compaction, temperature changes, melted water held within the snowpack, and addition of more fresh snow. (See Koren et al. (1999) for snow density formulations.)

Snow density was provided in the RUC GRIB output (but not in RAP) together with snow-water equivalent and snow depth. As calculated in RAP, snow density (kg m^{-3}) = Snow-water equivalent [kg m^{-2}] / snow depth [m].

HRRR/RAP uses the RUC land-surface model with a 2-level snow model (starting in 2011) and cold-season effects (freezing and thawing of moisture in soil - see Smirnova et al. 2016). The HRRR/RAP cycles snow depth/cover, as well as snow temperature in the top 5 cm and below that top snow layer. Fig. 22 shows snow-related variables from the HRRRX.
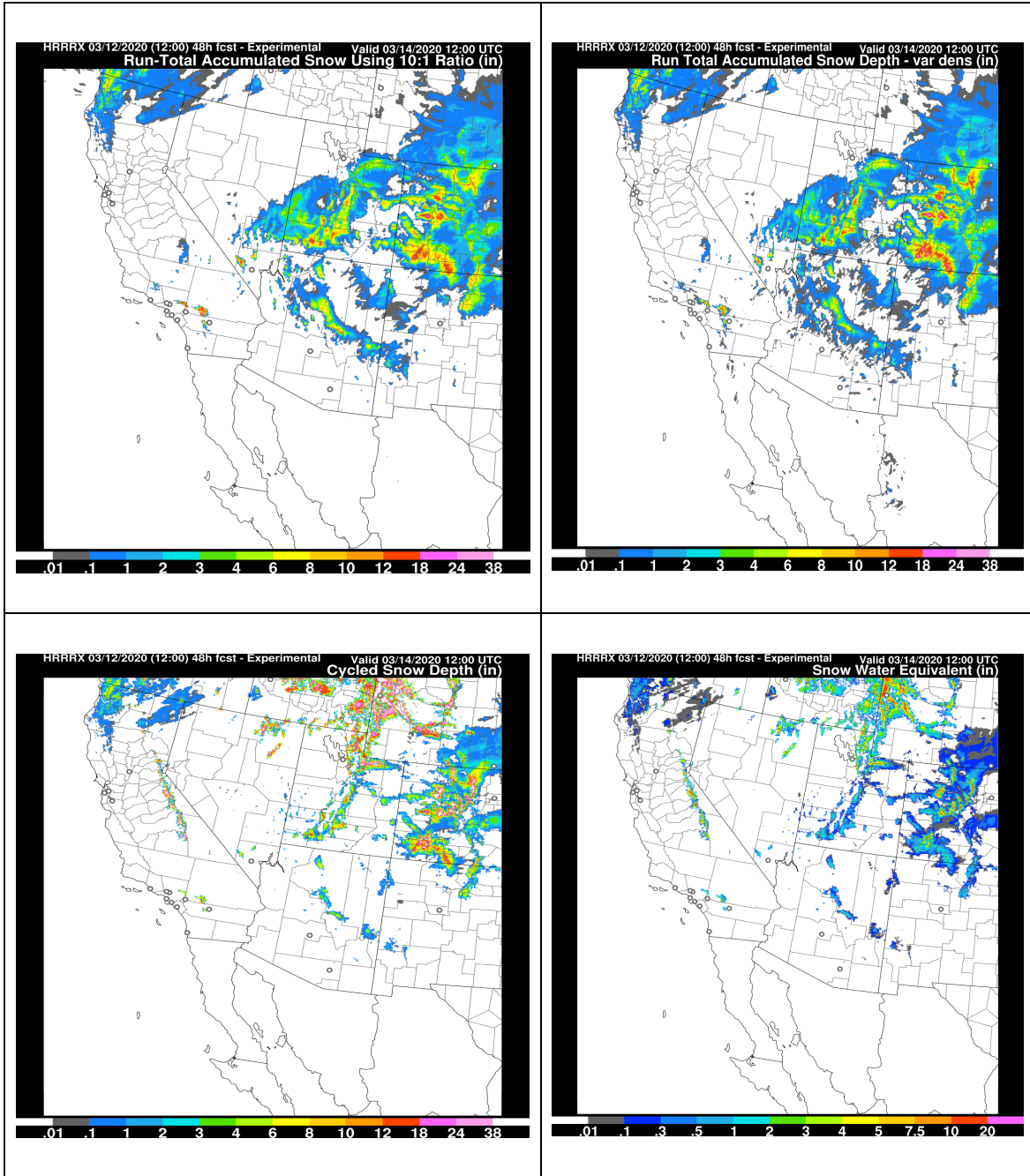
Fig. 22. Snow-related variables (all in inches) from HRRRX forecasts from the 12z/12 March run. **Accumulated snow applying a 10:1 ratio (upper left) and using variable density (upper right),** for the 48-h period ending 12z/14 March. Also, 48-h forecast valid at 12z/14 March of **snow depth (lower left) and snow-water equivalent (lower right).**

vii. Precipitation type(s) – potential area

Yes/no categorical indicators for rain, snow, ice pellets, and freezing rain potential are calculated from the 3-d hydrometeor mixing ratios reaching the ground calculated in the explicit Thompson cloud microphysics parameterization in the HRRR and RAP models. Details on the diagnosis of this explicit precipitation-type diagnosis were important and detailed enough to warrant a full journal article: Benjamin, Brown, Smirnova, 2016. A decision tree for the diagnosis is provided in Fig. 23, and an example forecast is shown in Fig. 24.

Summary: the p-type (precipitation type) values from this explicit diagnosis are not mutually exclusive; more than one value can be yes (1) at a grid point, just as with different hydrometeor species that can coexist at a given 3-d grid volume in the Thompson cloud scheme.   The accumulation thresholds used are very low, well below measurable thresholds, so the diagnostic will indicate **potential** areas of hazardous p-type conditions to increase the probability of detection and reduce unforecast hazardous events. It should be combined with QPF and freezing rain accumulation and sleet accumulation values.
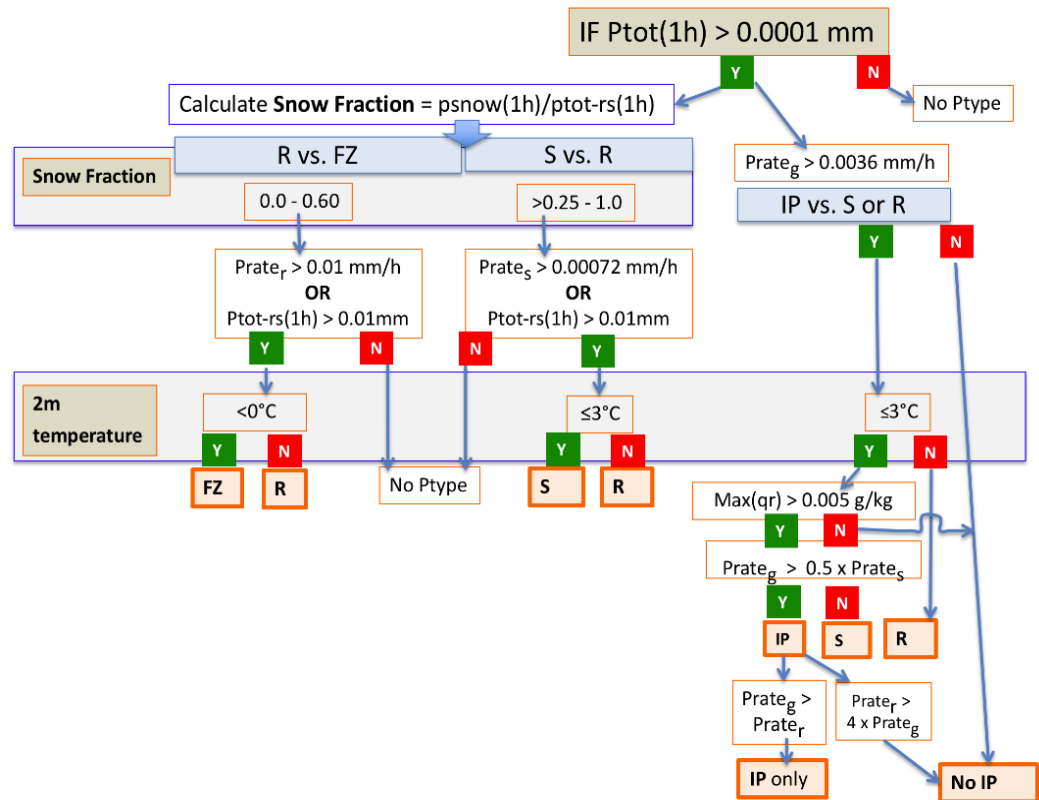
Fig. 23 - Explicit precipitation-type diagnostic method. From Benjamin et al. 2016b, Fig. 1. Flowchart describing the diagnostic logic for determination of precipitation type. (Bold letters in tan boxes: (**FZ, IP, R, S**) = (freezing rain, ice pellets, rain, snow). *Ptot*, *ptot-rs* and *psnow* are the total, rain plus snow (no graupel), and snow only (water-equivalent) precipitation, respectively, 1h indicating over the last hour. Prate is the instantaneous fall rate for different hydrometeor types (r – rain, s – snow, g – graupel). The maximum rain mixing ratio in the column is represented by Max(*qr*).

.01   .05   .1   .25   .5   .75   1   2
SNOW   FREEZING RAIN   RAIN   ICE PELLETS
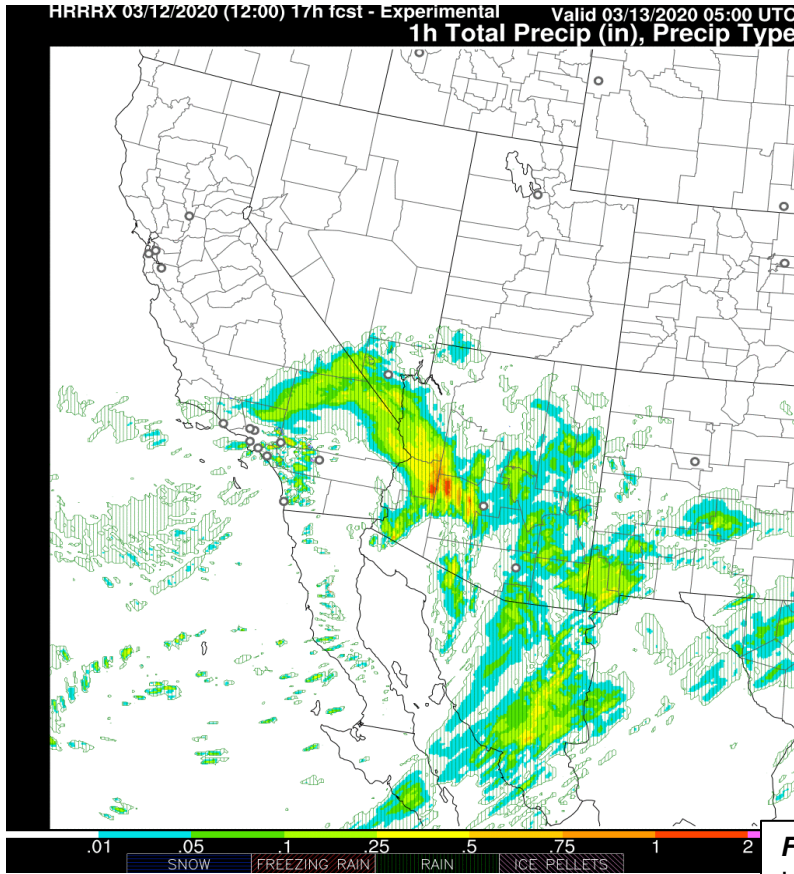
A change to RAPX and HRRRX was made to the ice-pellet diagnosis in Jan 2014, in which the integrated rain water requirement was changed from 0.05 g/kg to 0.005 g/kg. Prior to this change, ice pellets were rarely diagnosed. This modification was included in the operational HRRRv2/RAPv3 implementation in August 2016.

Fig. 24. Precipitation type. From 17-h HRRRX forecast valid at 05z/13 March combined with 1-h total precipitation (image) for the 1-h period ending at 05z/13 Mar.

viii. Maximum graupel/ hail size

The current HRRR output contains two diagnostics of maximum graupel/hail size (diameter) at the surface. The first diagnostic, which operates within the Thompson microphysics parameterization, calculates the maximum hail size directly from the calculated graupel size particle distribution. Beginning with HRRRv4, an additional hail diagnostic, referred to as HAILCAST (Adams-Selin and Ziegler 2016), based on a one-dimensional hail growth model is included in the HRRR output. Output from the two hail-size diagnostics is shown in Fig. 25 and 26.

Hail-related diagnostic fields from versions of HRRR model:

| HRRRv1/v2	Hourly max vertically integrated graupel
HRRRv3	Hourly max vertically integrated graupel Thompson MP-based hourly and vertical column maximum hail size diagnostic Thompson MP-based hourly maximum surface hail size diagnostic
HRRRv4	Hourly max vertically integrated graupel Thompson MP-based hourly and vertical column maximum hail size diagnostic Thompson MP-based hourly maximum surface hail size diagnostic HAILCAST (Adams-Selin) hourly maximum surface hail size diagnostic
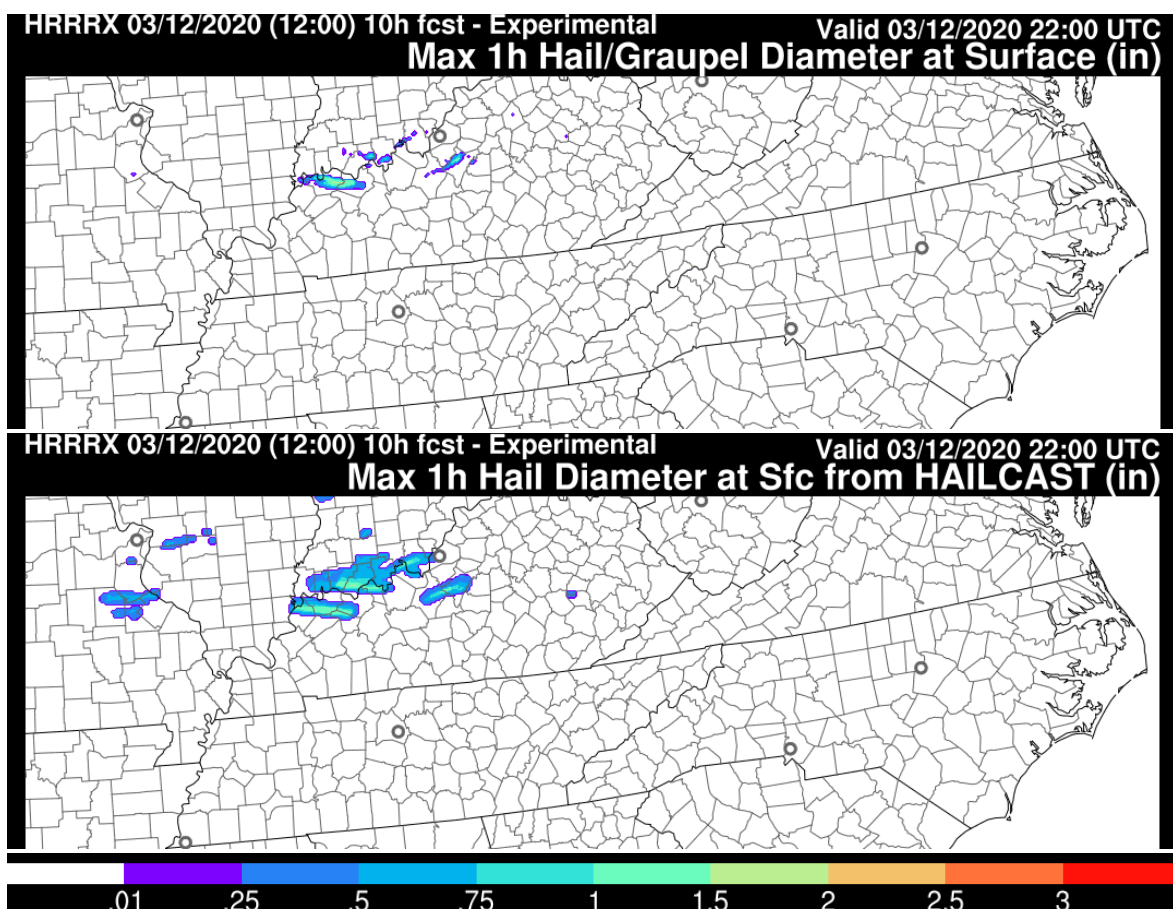
Fig. 26. Max hail/graupel diameter at the surface. 10-h Experimental HRRR 10-h forecasts from the 12z/12 March run valid at 22z/12 Mar at the surface for the 1-h ending at 05z (top), and maximum hail diameter using HAILCAST for the 1-h ending at 05z (bottom), both in inches, for a severe-weather event with accompanying supercell and other storms.

F. Severe-weather index variables

i. Lightning/thunder environment parameter. (Applicable to coarse-scale environmental data. Description for a different lightning diagnostic for convection-allowing models is described later.)

This thunder parameter (designed for environmental data from models using a convective parameterization) is from David Bright, formerly of the NOAA Storm Prediction Center. At any point where convective precipitation is forecast to occur (i.e., where the convective parameterization scheme is active), thunder is predicted if all of the following are true:
- The temp of the LCL is greater than -10°C
- The temp of the EL is less than -18°C
- The CAPE in the layer between 0 and -20°C exceeds 75 J kg^{-1}

This parameter is available in RAP only; the HRRR does not use a convective parameterization, rendering this parameter unnecessary. Additional information on the diagnostic is available at http://www.spc.noaa.gov/publications/bright/ltgparam.pdf

ii. CAPE/ CIN/ EL (equilibrium level)

Convective available potential energy (CAPE) is defined in RAP and HRRR using the standard Unipost definition of CAPE including use of virtual temperature. CAPE values are provided for surface-based CAPE, most unstable CAPE (MUCAPE) in lowest 300 hPa, and mixed-layer (lowest ~50 hPa mixed) CAPE (MLCAPE). The calculation of CAPE considers only positively buoyant contributions of the ascending air parcel, starting at the parcel's Lifted Condensation Level (LCL) and ending at the Equilibrium Level (EL).

Convective inhibition (CIN) indicates the accumulated negative buoyancy contributions for the ascending parcel, starting at the parcel's LCL and ending at its EL. By this definition, CIN is mainly accumulated between the LCL and the Level of Free Convection (LFC), and represents the negative buoyant energy that must be overcome in order for the parcel to become positively buoyant once it reaches its LCL. This is also the standard Unipost definition.

Equilibrium level (EL) indicates the highest positively buoyant level. This is also the standard Unipost definition. The EL provided is associated with the most unstable CAPE parcel (MUCAPE; using the parcel with highest θ_e in the lowest 300 hPa).

Examples of the different CAPE and CIN variables are shown below (Figs. 27-28) for the southeast map domain from the HRRR website for a case of severe convection using forecasts from the 12z/12 March 2020 HRRRX run.
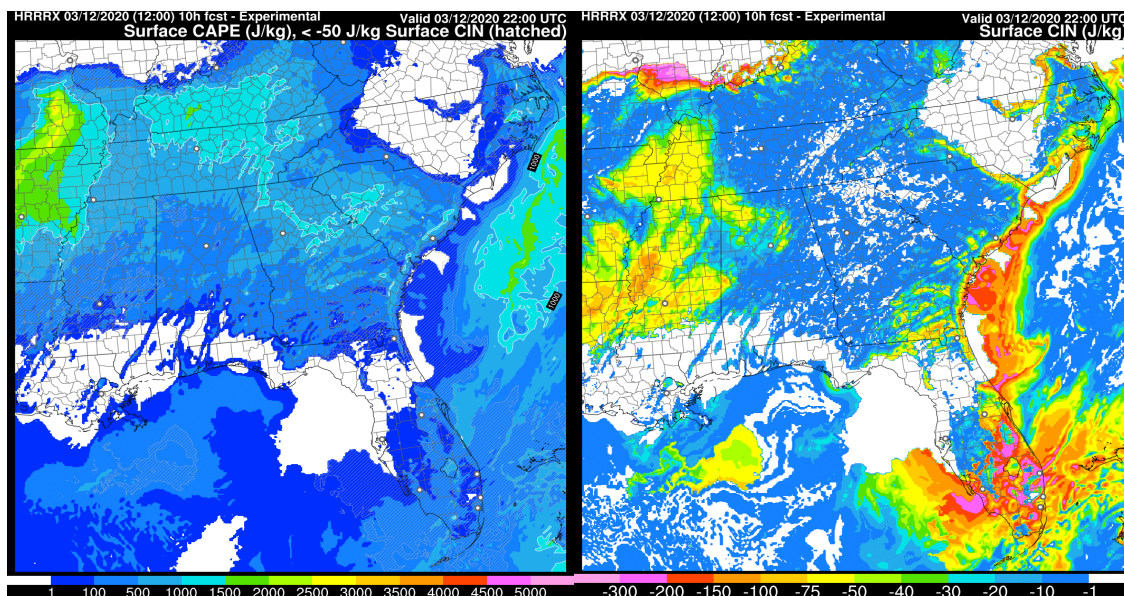

Fig. 27. CAPE/CIN variables. 10-h Experimental HRRR 10-h forecasts from the 12z/12 March 2020 run valid at 22z/12 Mar for (left) a combination of surface-based CAPE (image) with surface-based CIN (faint diagonal hatching for values less than -50 J/kg) and (right) for CIN only.
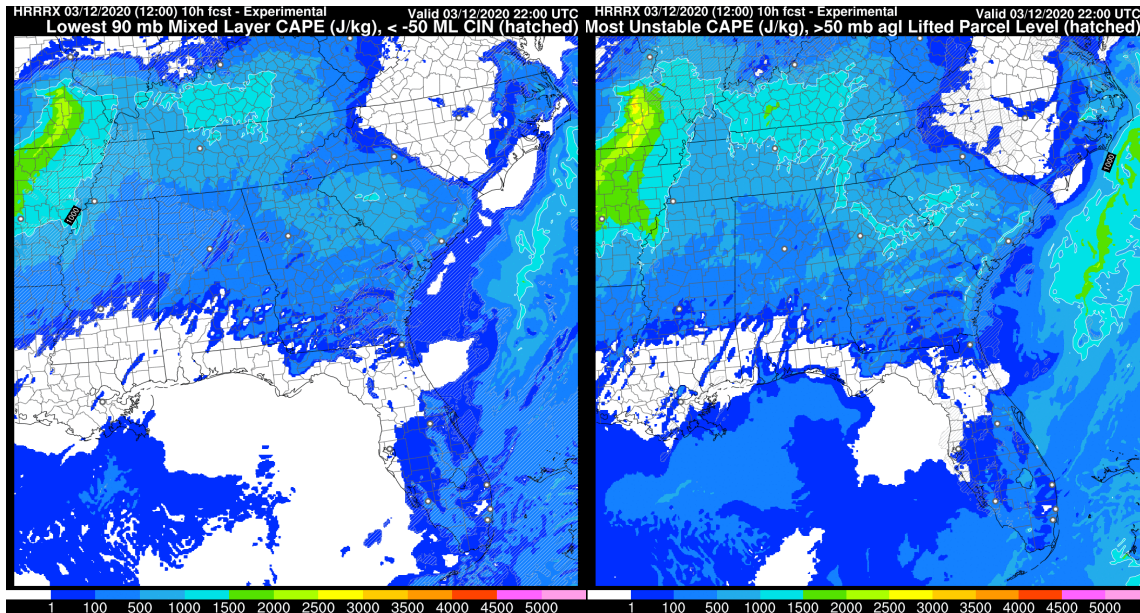
Fig. 28. Other CAPE and CIN variables. Top left figure shows an image for the **mixed-layer CAPE** with the mixed layer from the lowest 90 hPa, along with hatching where CIN has values below (greater than) -50 J/kg. Top-right figure has an image for the **most-unstable CAPE** at any point in the atmosphere below the 300-hPa level with hatching if that point is above the lowest 50 hPa of the atmosphere (this distinguishes elevated instability from lower level or surface-based CAPE). Both figures show 10-h forecasts from the 12z/12 Mar HRRRX.

iii. Lifted index (LI)

The lifted index (Fig. 29) indicates the difference between environmental temperature and ascending parcel temperature at 500 hPa (in K). The standard lifted index uses the surface parcel, and best lifted index uses the buoyant parcel from the native level with maximum buoyancy within 300 hPa of surface (also the standard Unipost definition).
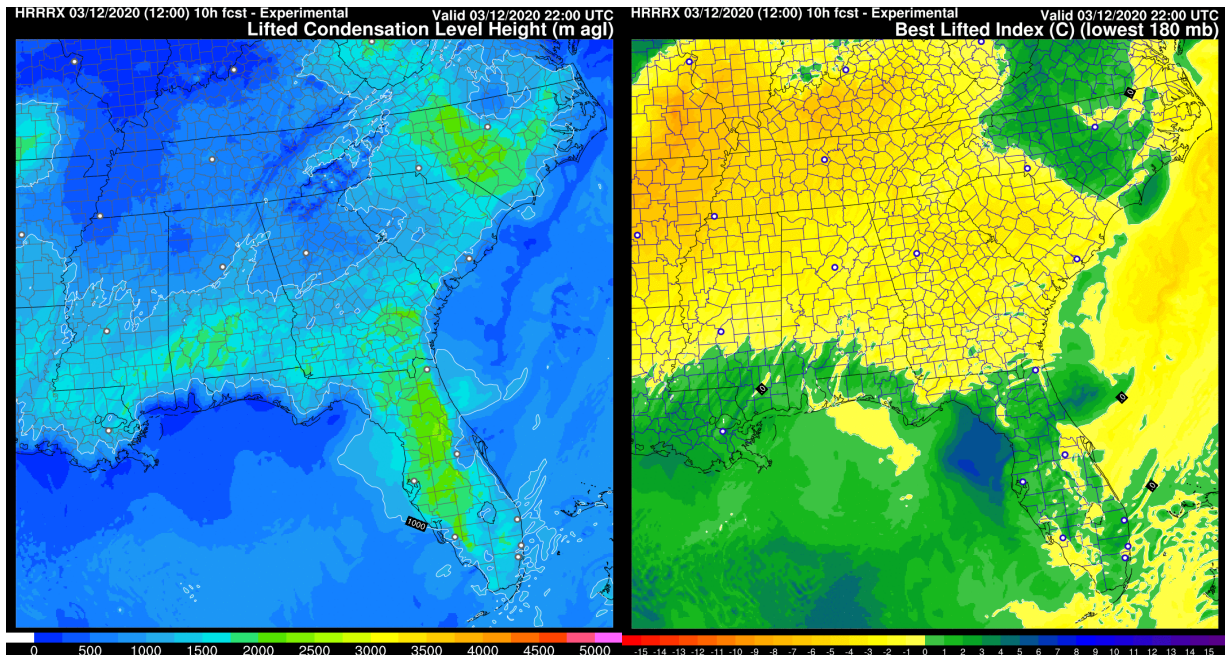
Fig. 29. LCL (left) and LI (right). 10-h HRRRX forecasts from the 12z/12 March 2020 run valid at 22z/12 Mar of Lifting Condensation Level (LCL, in m AGL, on left). Best Lifted Index (LI, ⁰C, using the best parcel in the lowest 300 hPa (caption incorrect) of the atmosphere) on right.

iv. Environmental helicity/storm motion

Environmental (not *storm-relative*) helicity and storm motion are defined following the diagnostics of Bunkers et al. (2000). Examples of vertical wind shear are shown in Fig. 30, and storm-relative helicity and storm motion in Fig. 31.

What can be considered high values of environmental helicity?
The units of helicity are $m^2 s^{-2}$. The value of 150 $m^2 s^{-2}$ is generally considered to be the low threshold for tornado formation. Helicity is basically a measure of the low-level shear, so in high-shear situations, such as behind strong cold fronts or ahead of warm fronts, the values will be very large, possibly as high as 1500 $m^2 s^{-2}$. High negative values are also possible in reverse shear situations.

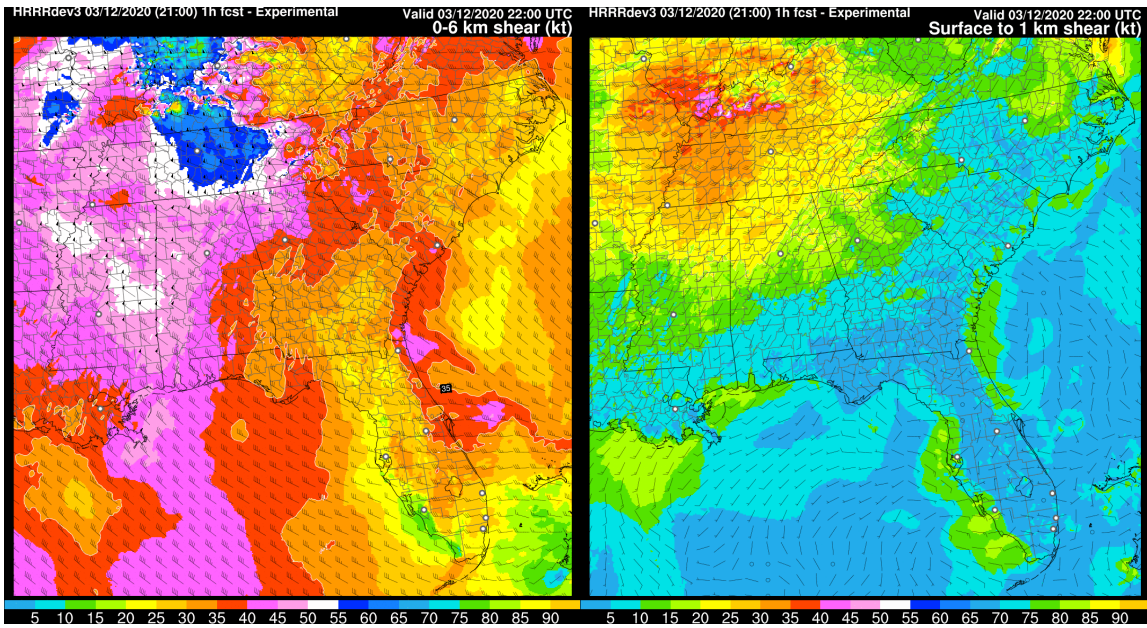**Fig. 30. 0-6 km (AGL) shear (left) and surface to 1 km AGL shear (right),** both in knots. Shown are 1-h forecasts from an experimental version of the HRRR valid at 22z/12 March.
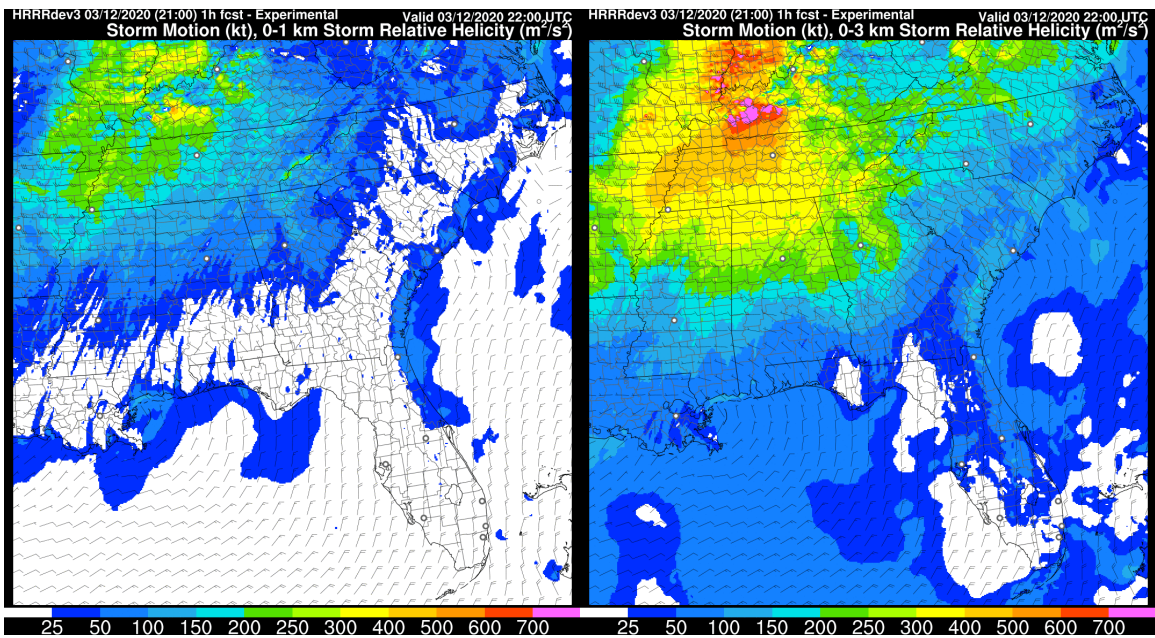

Fig. 31. Storm-relative helicity (SRH, in m^2/s^2) fields displayed with calculated storm motion. 0-1 km AGL SRH (left) and surface-to-3km AGL SRH (right). Shown are 1-h forecasts from HRRRX valid at 22z/12 March.

G. Cloud-related variables

i. Cloud-base height and ceiling (2 separate, related fields for HRRR and RAP)

General information for both fields:
- Units - meters above sea level (ASL). Note that the RAP/HRRR graphics show cloud base above GROUND level (AGL) -- the RAP/HRRR terrain elevation height is subtracted first. But in the actual GRIB files, cloud base height is in ASL.
- In GRIB - Horizontal grid points without any cloud layer are indicated with -99999.
- **Recommended - use 'ceiling' field, not 'cloud-base field',** as described further below.

In general, the ceiling diagnostic consists primarily of the lowest level with cloud water or ice mixing ratio (explicit clouds) exceeding a small threshold combined with a second condition using near-saturation RH at the PBL top (conditions 1 and 3, below). But other important details, including the history of the ceiling diagnostic, are described below.

The diagnostics for ceiling or cloud-base height use a combination of different diagnostic conditions listed below. Here are those conditions which have been used in some combination for the RAP/HRRR models, depending on version (Table 1). Conditions 1-4 were developed originally with the RUC model in the 2000s.

Conditions:

1. Lowest model level (searching from surface upward) at which combined cloud water (qc) and ice (qi) mixing ratio exceeds 10^{-7} g g^{-1} (Condition #1). A vertical interpolation between levels is performed, so this condition gives a continuous value. This interpolation depends on how much the cloud water/ice mixing ratio exceeds the limit at the first level encountered.
2. Lowering of ceiling from falling snow. This corresponds to the "vertical visibility" sometimes reported in METAR reports. This condition uses the visibility calculation based on snow mixing ratio.
3. PBL-top cloud-top ceiling diagnosed from PBL-top RH. If PBL-top RH > 95%, a ceiling is identified at this level even if there is no explicit cloud water or ice at this level. Note: this Condition #3, while crude, has been a critical addition even for the 3km HRRR scale.
4. Avoid identifying surface fog layers as low ceiling. If cloud water is available at level 2 (~32 m AGL) and/or level 3 (~80 m AGL) but not above that level, this is ascribed as a fog layer near the surface too shallow to be an aviation-affecting ceiling.
5. Use of explicit subgrid cloud fraction (from MYNN boundary-layer scheme) with a threshold of 0.4-0.5. (New in 2020 with HRRRv4/RAPv5)

Starting 2016 (RAPv3/HRRRv2):
- Ceiling height for RAP and HRRR uses the combination of Conditions 1-4 (more cloud/ceiling detection than Condition 1 alone, especially with the addition of Condition 3).
- Cloud-base field (through RAPv4/HRRRv3) uses only Condition 1. This **"cloud base" field should NOT be used for ceiling (especially for aviation forecasts) and instead, always use the "ceiling" field from RAP and HRRR GRIB grids.**

- Starting with the operational HRRRv4/RAPv5 (2 Dec 2020), the "cloud-base height" variable is switched to use Condition 5, replacing the previous Condition 1. This is considered to be an experimental ceiling diagnostic, not yet as effective as the existing (legacy) ceiling in the cold season (excessive) but
- **NOTE**: Before 2016, the opposite was true for the RAP - the best estimate of ceiling using Conditions 1-4 was in the field labeled as the "cloud base" field.

Starting May 2020 (HRRRv4/RAPv5): "Ceiling" continues to use Conditions 1-4. But now, the "cloud-base height" variable uses only the new Condition 5 (explicit subgrid cloud fraction - Olson et al 2019b). (See table below.). Examples are shown in Fig. 32.
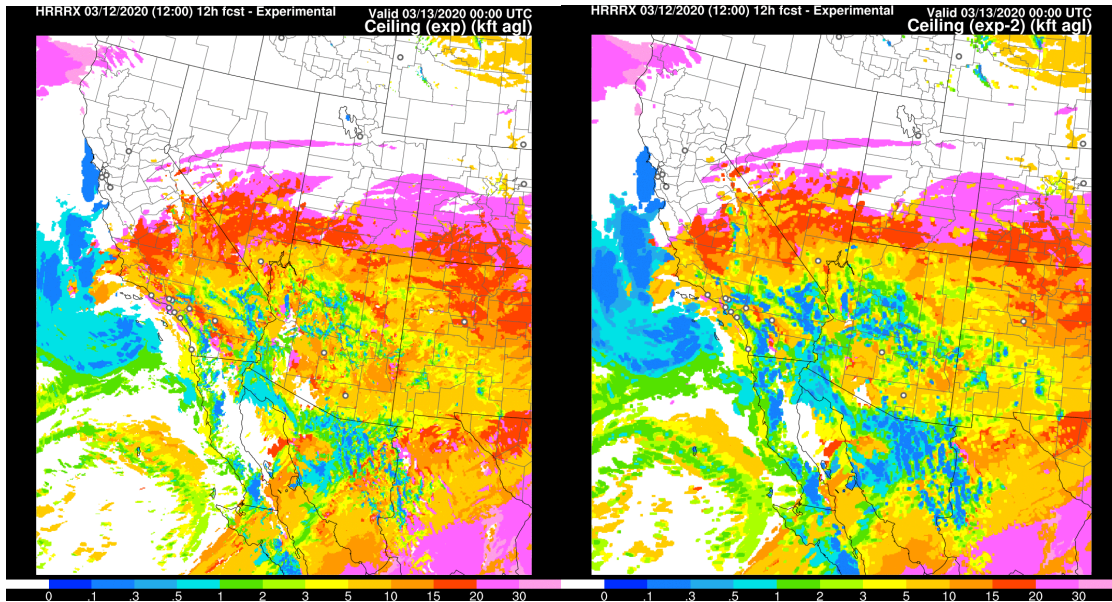

Fig. 32. Ceiling using conditions 1-4 (left). Cloud-base diagnostic (using condition 5 using semi-prognostic cloud fraction, new as experimental in HRRRv4 - right). Both are for 12-h HRRRX forecast valid 00z 13 March 2020. Units for both: height above the surface (AGL) in thousands of feet (kft).

Conditions for ceiling-related diagnostics	**Ceiling**	**Cloud-base**
RAPv1-v4, HRRRv1-v3	Conditions 1-4	Condition 1 only
RAPv5, HRRRv4	Conditions 1-4	Condition 5 only (experimental)

ii. Cloud-top height
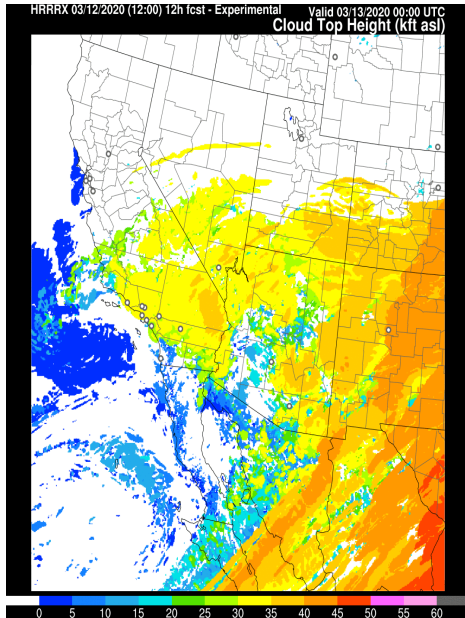
Cloud-top height (Fig. 33) is defined as the top model level at which combined cloud-water and ice mixing ratio exceeds 10^{-6} g g^{-1}. Units are meters above sea level, and horizontal grid points without any cloud layer are indicated with -99999.

Fig. 33. *Cloud-top height.* 12-h forecast of (kft above sea level) from the 12z/12 March HRRRX valid at 00z/13 Mar

iii. Cloud fraction

The cloud-fraction diagnostic has evolved over the years – data from older versions are not recommended for many applications, but that from HRRRv4/RAPv5 is of better quality. By an earlier requirement from NWS, output from the cloud-fraction has been traditionally provided as the **maximum** layer-column value from native model levels for three layers: a low-level layer (up to 840 hPa), mid-level layer (842-350 hPa), and high-level layer (above 350 hPa).

Prior to 2014, in the RAP, this field was, generally, either 0 or 100% since non-zero cloud hydrometeor mixing ratios can only occur if the grid volume is saturated, but includes some horizontal smoothing not in the RUC.

Since 2014 (HRRRv1) until HRRRv3 (see Table 1), cloud fraction was a strongly smoothed field using a 40-km-radius smoother. This field will not produce accurate downward solar radiation or other grid-point-specific cloud fields.

Beginning in 2019/2020, HRRRv4/RAPv5 now calculates cloud fraction from the semi-prognostic subgrid cloud fraction from the MYNN PBL scheme (Olson et al. 2019a,b), allowing for much more realistic cloud fractions for low and mid-level clouds (see Fig. 34). This cloud fraction may not be accurate from an individual gridpoint for an instantaneous comparison at an individual location but will have more accuracy averaged over local zones and over short time intervals. In addition, HRRRv4/RAPv5 has added a *boundary-layer cloud fraction field*, which we recommend using instead of the low-level cloud fraction (which is not usable for areas with elevated terrain). This cloud fraction for this layer (diagnosed PBL depth plus 1 km) is the maximum value in the column for native levels within this layer.
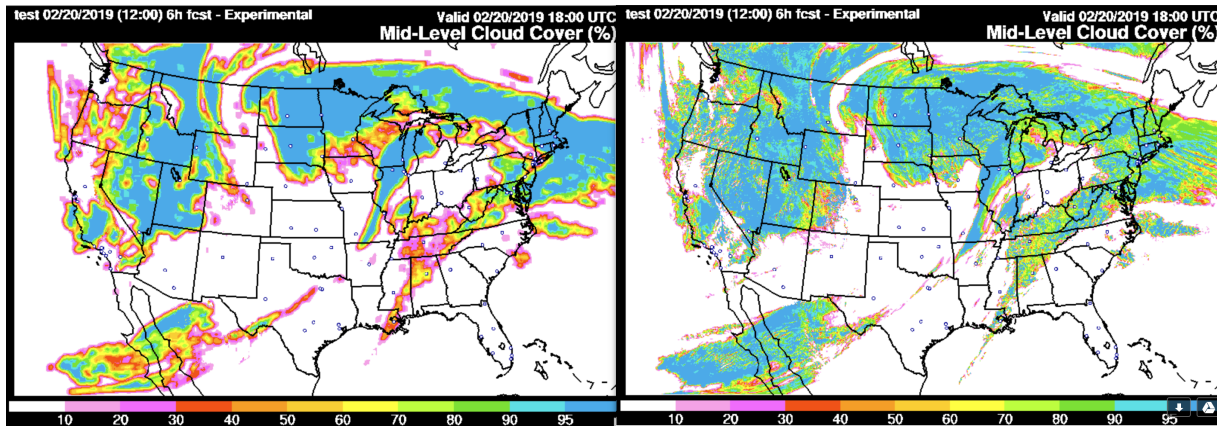
Fig. 34. Mid-level cloud cover (%) from (left) the old (HRRRv1-v3) smoothed diagnostic and (right) the new diagnostic taking advantage of MYNN sub-grid scale clouds in HRRRv4/RAPv5. The forecast is a 6-h forecast valid at 18 UTC 20 Feb 2019.

iv. Surface visibility

The surface visibility algorithm developed for and used in RUC/RAP/HRRR is an extension of the Stoelinga-Warner (JAM, 1999) algorithm designed to take advantage of explicit hydrometeor types used in those models (Fig. 35). It is usable for any model with explicit hydrometeor predictions.

This visibility diagnostic is based on conditions at the lowest model level (about 8 m AGL) for these variables:

Fig. 35. Surface visibility (in miles). 12-h forecast from the 12z/12 March 2020 HRRRX, valid at 00z/13 Mar.

- Non-zero hydrometeors, with attenuation coefficients for each hydrometeor type (qc, qi, qr, qs, qg). Maximum value of each hydrometeor type is calculated from the lowest 3 layers (from 6-8m AGL up to 60-75m AGL for RAP and HRRR).
- day/night dependency for hydrometeor attenuation coefficients from Roy Rasmussen (NCAR, 2000)
- additional visibility attenuation term for forecast graupel hydrometeor mixing ratio
- additional relative humidity dependency developed by RUC/RAP group using max RH at the lowest 2 levels. This RH term approximates the effects of haze on visibility. It allows a maximum 90-km (~56 mile) visibility with near-surface RH <15% and a
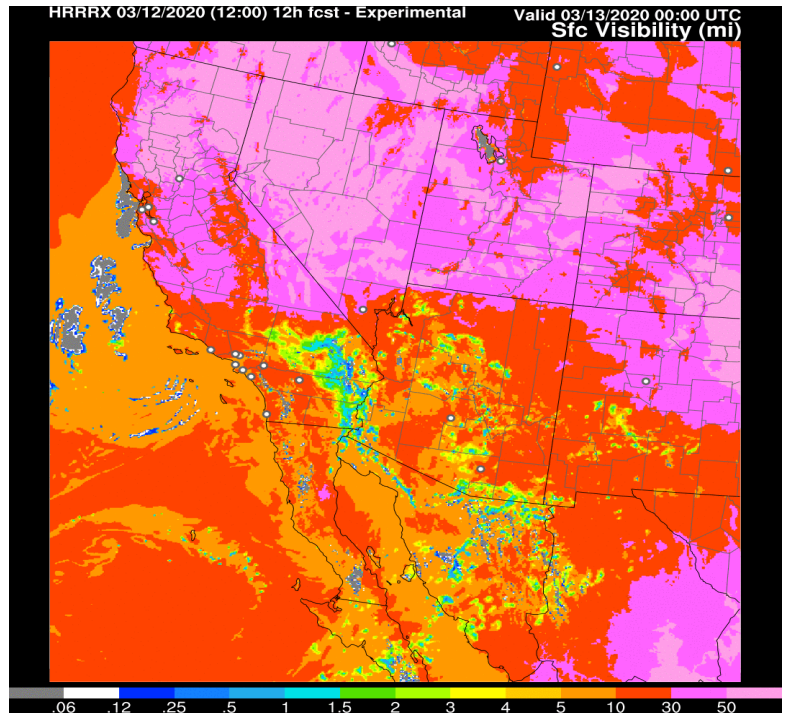
minimum ~12-km (~7 mile) visibility with near-surface RH >95%. (Modified starting with RAPv4/HRRRv3 to reduce estimated attenuation from haze.)
- smoke extinction (from 3-d smoke concentration at lowest level, if available) is included beginning with RAPv5/HRRRv4 (2020).

Generally, if hydrometeors are present at either of the two lowest levels (~6-8m and ~25-30m AGL), the diagnosed visibility will be less than 5-6 miles and usually, less than 3 miles. Otherwise (for estimated visibility > 7 miles), near-surface RH largely governs the visibility estimate. The inclusion of smoke effect is accomplished by assigning the overall surface visibility as the minimum of visibility from hydrometeors and smoke combined (each with their own extinction coefficients) vs. the visibility from RH.

v. Simulated satellite imagery

Beginning with the HRRRv2, implemented at NCEP in August 2016, the HRRR has output synthetic simulated satellite imagery in the thermal infrared band (10.7 micron wavelength; Fig. 36) and the water vapor band (6.5 micron wavelength; Fig. 37), which is intended for comparison with satellite observations from GOES-East and GOES-West. The simulated brightness temperatures are computed using the HRRR output and the Community Radiative Transfer Model (CRTM; Han et al. 2006). The calculations take into account the correct viewing geometry of GOES-East and GOES-West. The brightness temperature of clear grid points is calculated based on surface skin temperature, 10-m wind speed, pressure, and vertical profiles of temperature and water vapor. The brightness temperature of cloudy grid points uses vertical profiles of mixing ratio and number concentration for each hydrometeor species included in the Thompson-Eidhammer aerosol-aware microphysics scheme (Thompson and Eidhammer 2014). (Unfortunately, the simulated satellite images do not include effects from subgrid-scale clouds (Olson et al 2019a).) Additional details about the formulation of the simulated brightness temperatures is provided by Griffin et al. (2017) and Otkin et al. (2007). **Note**: These simulated images are for the pre-GOES-R channels (i.e., from GOES-12, -13, -14, and -15). The new GOES-R (GOES-16 and -17) and old GOES-East/West IR channels are about the same, (now 10.3 microns vs. the old 10.7 band.
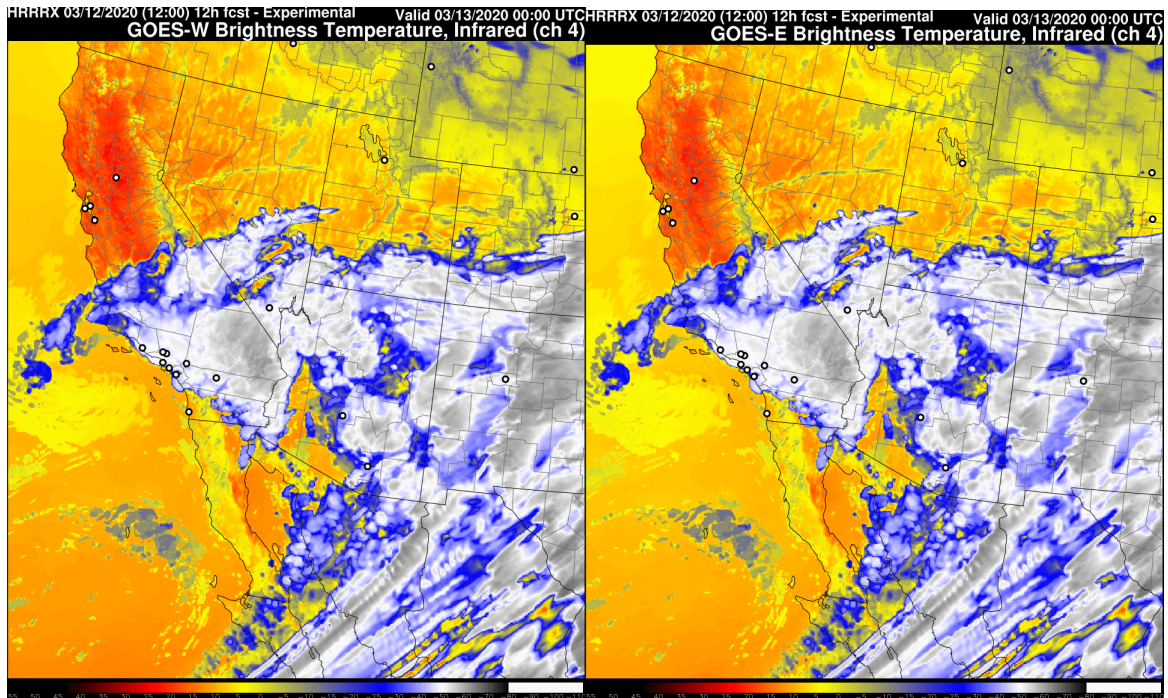
Fig. 36. Simulated IR imagery. 12-h forecasts from the 12z/12 March HRRRX valid 00z/13 March, simulating the view from GOES-W (left) and GOES-E (right).
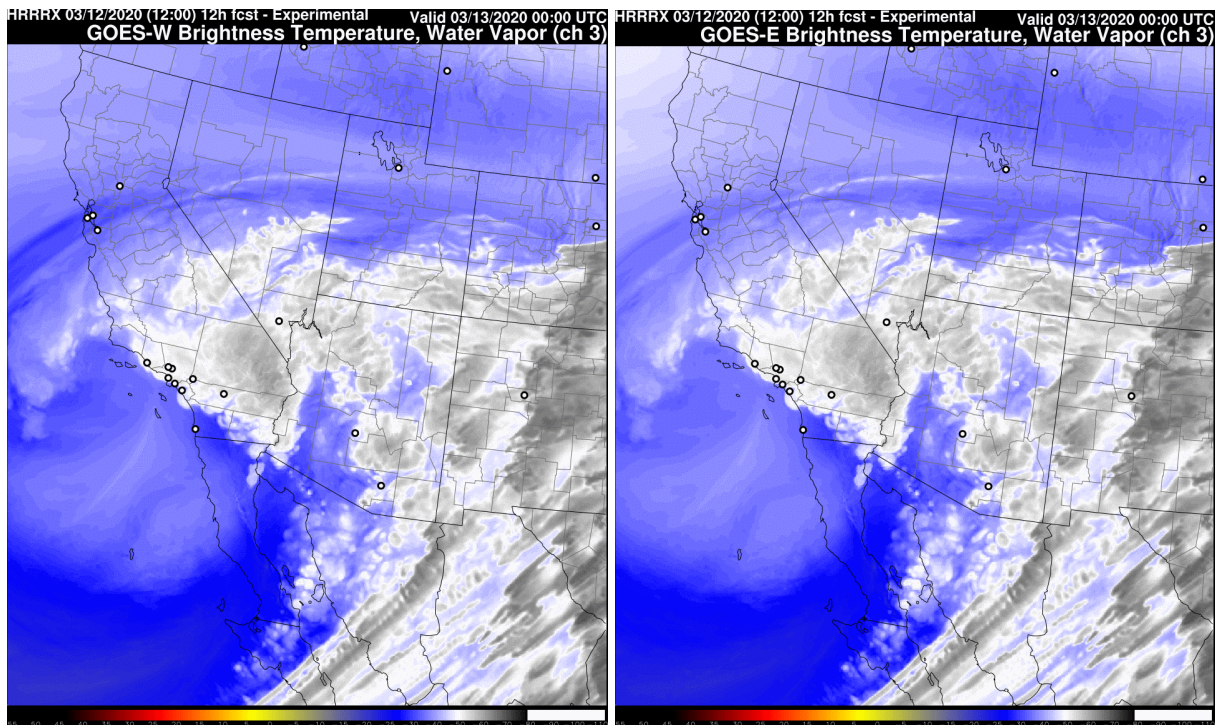

Fig. 37. Simulated water-vapor imagery. From the 12z/12 March HRRRX 12-h forecast valid 00z/13 March, simulating the view from GOES-W (left) and GOES-E (right).

### H. Explicit-scale convective-storm variables

i. Radar reflectivity

Radar reflectivity products are produced in a different manner for hourly/15-min instantaneous and hourly maximum fields. For **instantaneous** fields with hourly or 15-min output, reflectivity is calculated using a **more sophisticated** method within the Thompson scheme for each model 3-d grid point based on rain, snow, graupel/hail, and temperature at that grid point. The temperature is used to determine if melting snow is present (i.e., if there should be a "bright band" in the computed reflectivity).

These reflectivity diagnostics are produced:
- Composite reflectivity (maximum reflectivity in model column)
- 1-km AGL reflectivity (interpolated in model to 1-km AGL level)
- -10°C reflectivity.

Hourly maximum fields using timestep-by-timestep calculations are produced for 1-km AGL and -10°C reflectivity diagnostics. For these hourly maximum values, a **simpler** reflectivity diagnostic, not internal to the Thompson scheme, is applied. Examples are shown in Fig. 38.
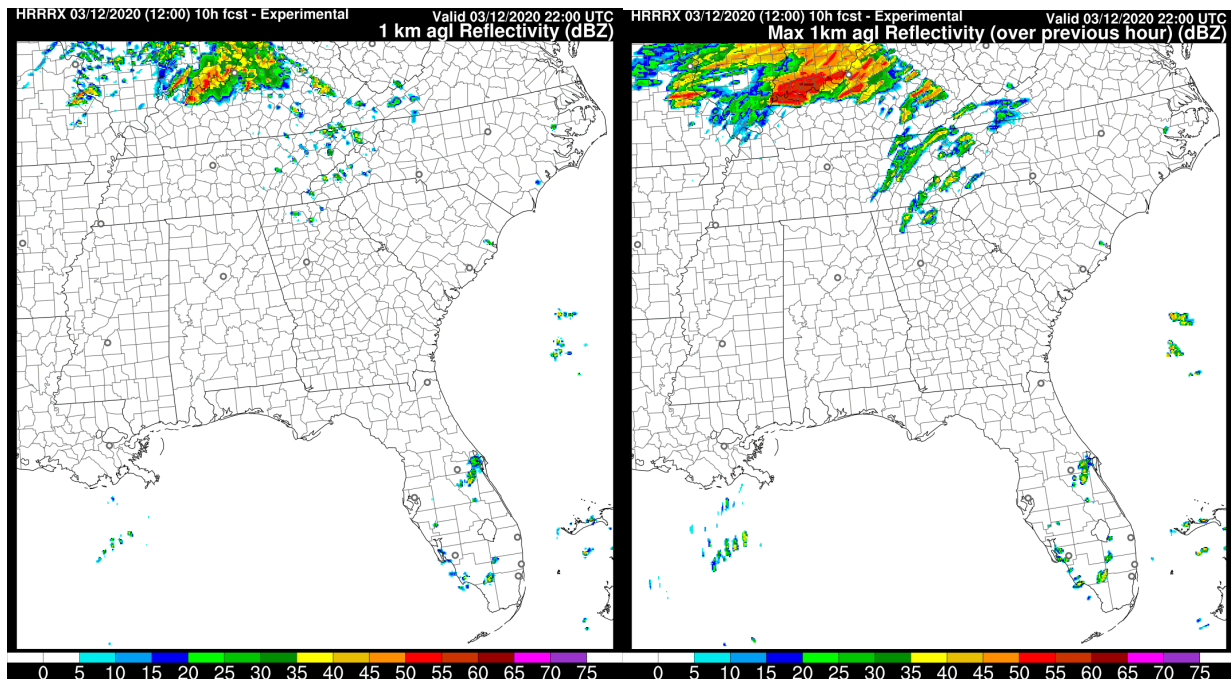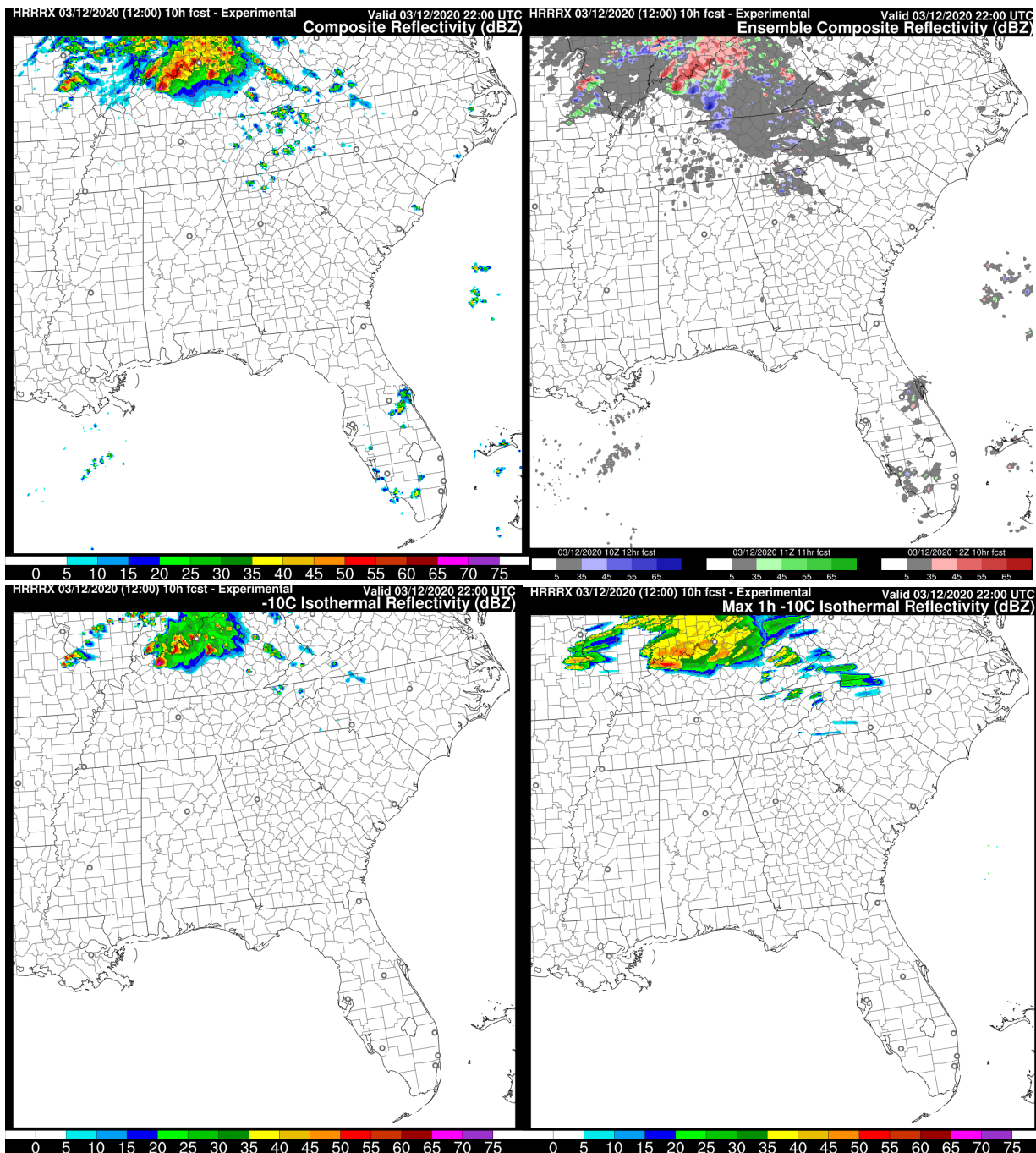
***Fig. 38. Reflectivity fields.* (Units - dBZ).** All are 10-h forecasts from the 12z/12 March HRRRX valid 22z/12 March. **Top row** displays two types of reflectivity at the 1-km AGL level, (upper left) instantaneous reflectivity at the forecast time (here 22z) and (upper right) maximum reflectivity over the previous hour (1-h ending at 22z). **Middle row:** (left) composite reflectivity, and (middle right) time-lagged ensemble composite reflectivity. This time-lagged ensemble combines forecasts from the current run (12z) and the previous two runs (11z and 10z runs) are displayed on the same figure, all valid at 22z, using different colors for each run (and highlighting values greater than 35 dBZ). In the **bottom row:** two types of reflectivity interpolated to the -10°C level are displayed, similar to the 1-km reflectivity in the top row.

ii. Lightning diagnostic (for convection-allowing model output with explicit microphysics)

Hourly maximum lightning threat is a measure of total lightning (cloud-to-ground and in-cloud). It is calculated for each model column based on the vertically integrated ice (cloud ice, snow, graupel) and the vertical graupel flux (vertical motion and graupel) (McCaul et al., 2009). The units are flashes per square km every 5 minutes; Fig. 39). It attempts to capture both lower frequency, broad anvil lightning and higher frequency lightning near updrafts. The McCaul scheme consists of two algorithms ("Threat 1" and "Threat 2") that are combined to produce a blended lightning, Threat 3.

Threat 1: Graupel Flux at -15°C. This is the product of qg and w, where qg is the predicted mixing ratio of graupel, and w is the vertical velocity, both interpolated to the level where the temperature is -15°C. This can be looked at as an estimate of charge separation produced in an updraft. This is done for each horizontal grid point, to produce a horizontal map of Threat 1.

Threat 2: Vertical Ice Integral. This is the vertical integral of all ice hydrometeors at each horizontal grid point. The ice hydrometeors in the HRRR (from the Thompson scheme) are qi (cloud ice), qs (snow), and qg (graupel). This threat diagnostic is an attempt to capture the lightning threat from thunderstorm anvils, where vertical motions are weak, but a considerable concentration of charged ice particles may be present aloft.

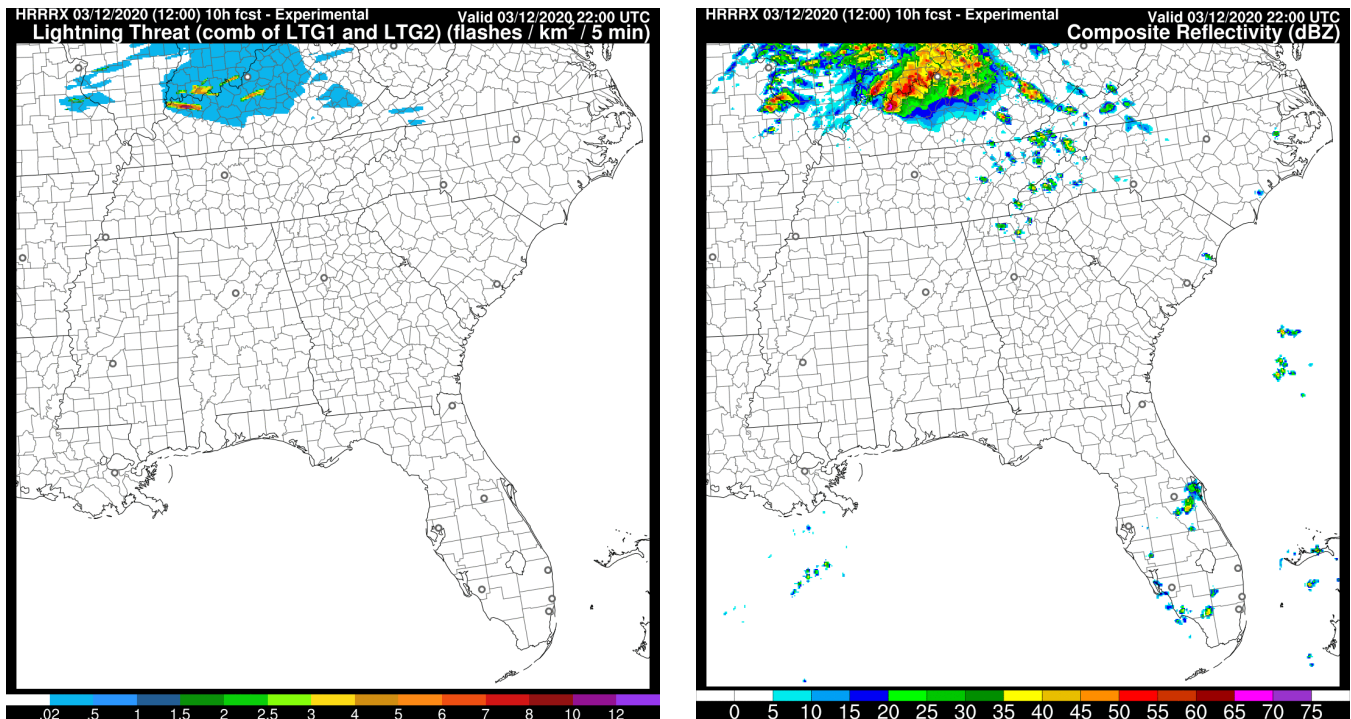Threat 3 = a * Threat 1 + b * Threat 2, where a and b are empirically determined weights.

Fig. 39. Lightning Threat using McCaul diagnostic. 10-h forecast valid at 22z/12 Mar from the 12z/12 Mar HRRRX, compared to composite reflectivity from the same forecast on right.

iii. Updraft helicity

Hourly maximum and minimum updraft helicity (UH) are calculated as hourly maxima or minima valid at the end of each hour. UH is derived from upward vertical velocity and cyclonic vertical vorticity in a given vertical layer; HRRR maximum and minimum UH are diagnosed between 0 and 2 km, 0 and 3 km, 2 and 5 km, and 1 and 6 km AGL. In cases where the lower boundary is at 0 km AGL, the 10-m wind field is used as the wind at the lower boundary. UH indicates updraft rotation in forecasted convection, which can imply a threat for tornadoes but does not explicitly predict tornadoes. UH maxima identify cyclonic rotation, while minima identify anticyclonic rotation. Since UH depends partially on updraft strength, it can be small in low CAPE, highly sheared environments. It does not discriminate between elevated and surface-based convection.
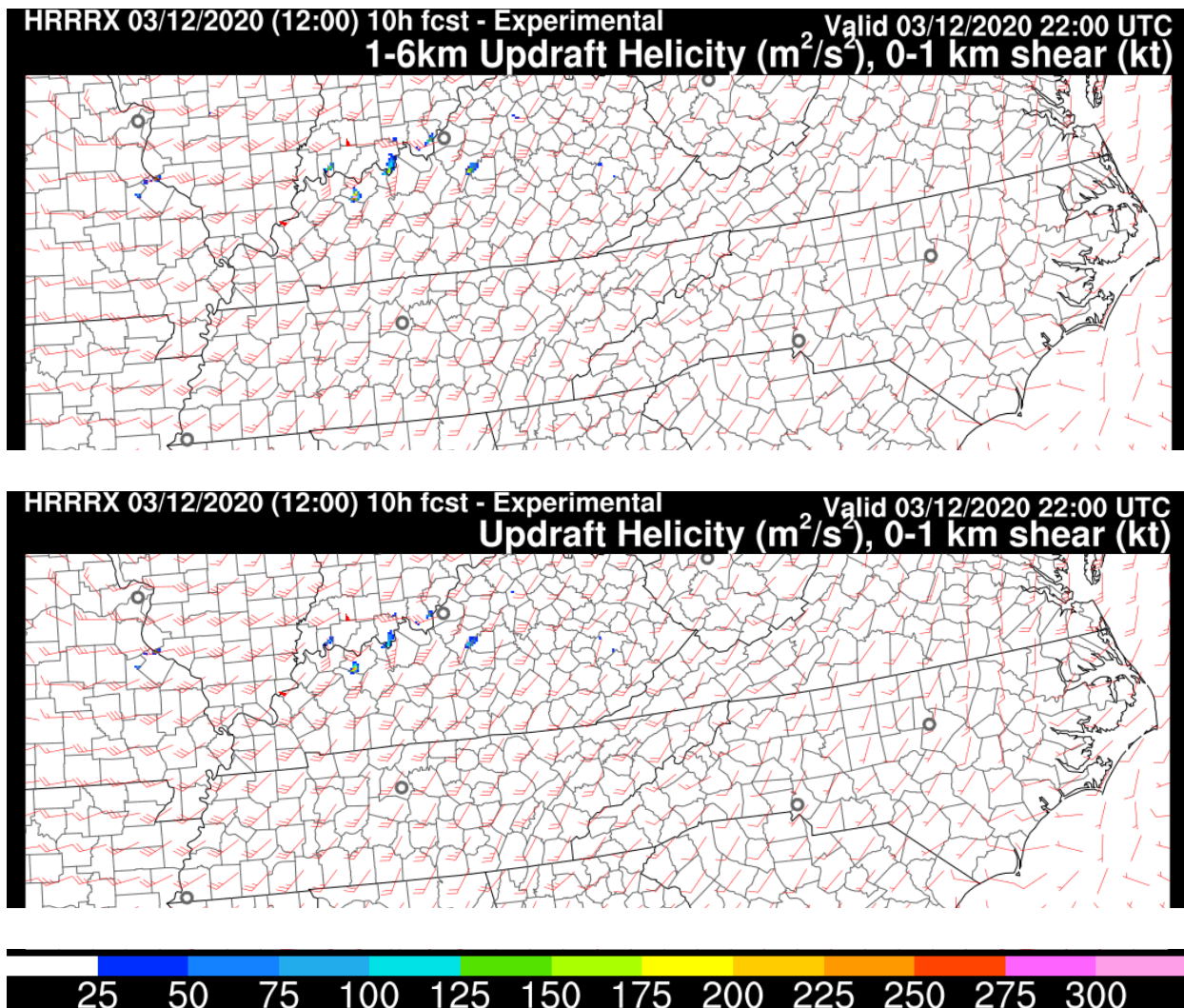

Fig. 40. Updraft helicity (UH - _Instantaneous_ values, in m²s⁻²). Shown here from the HRRR website for two levels, displayed with 0-1 km vertical shear vector (wind barb). Top image is for

the 1-6 km UH and the bottom image for the 2-5 km UH. Both are 10-h forecasts valid at 22z/12 Mar from the 12z/12 Mar HRRRX for a severe weather event.
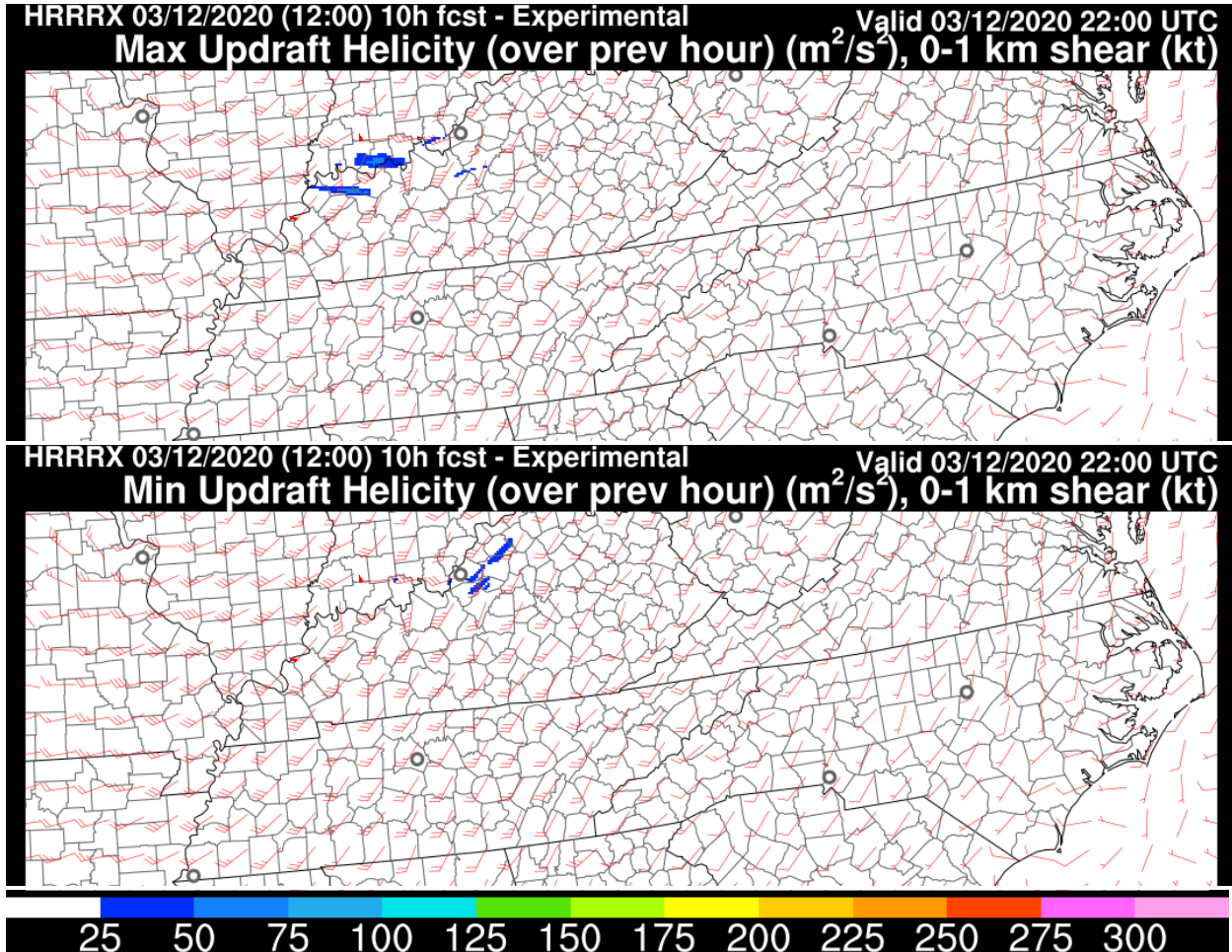

Fig. 41. Maximum/minimum updraft helicity (m^2s^{-2}) over previous 1-h period. Also shown - 0-1 km vertical shear vector (wind barb). These UH values are displayed for several vertical intervals, with displays for max UH over the previous hour to show UH tracks for cyclonically rotating model storms ("*right-movers*") and min UH over the previous hour to show UH tracks for *anticyclonically* rotating model storms ("*left-movers*"). For 10-h forecasts valid at 22z/12 Mar for the 0-1 km shear and for the 1-h ending at 22z for the UH, from the 12z/12 Mar HRRRX.

HRRRX 03/12/2020 (12:00) 10h fcst - Experimental
Ensemble Max Updraft Helicity (over prev hour) (m²/s²)
Valid 03/12/2020 22:00 UTC

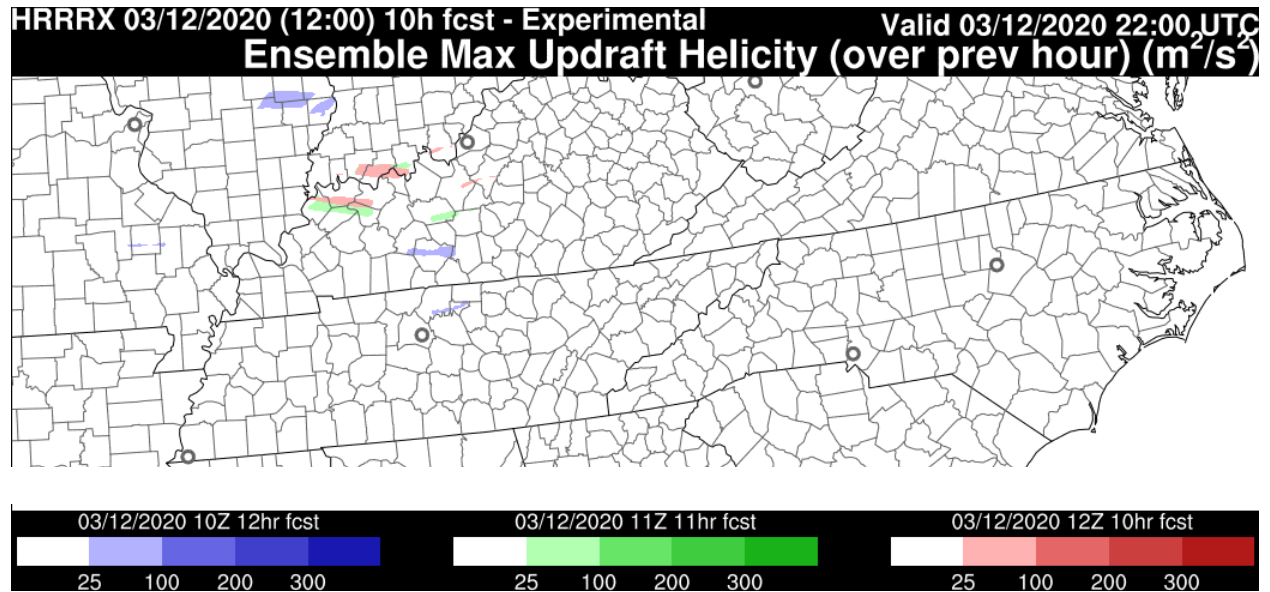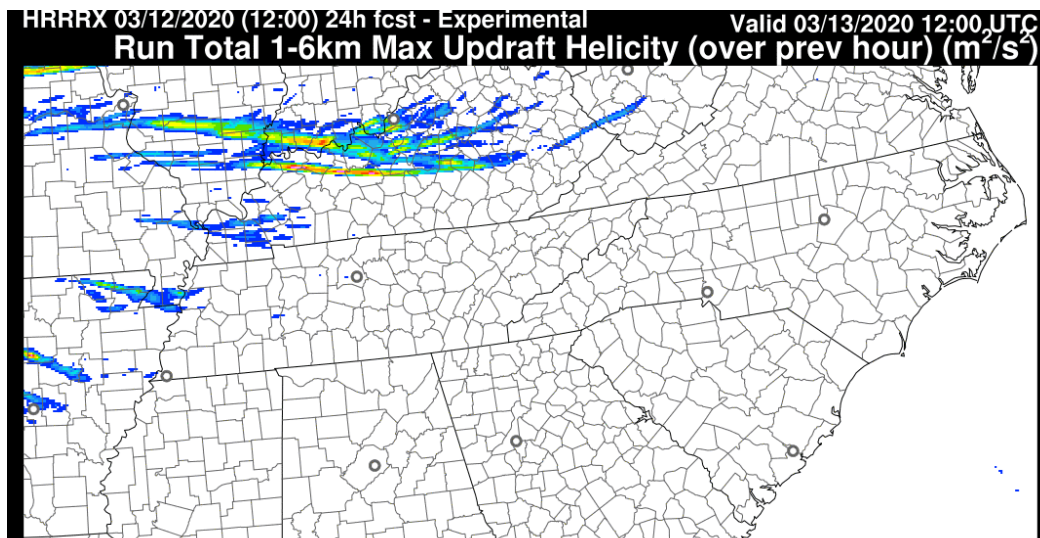| 03/12/2020 10Z 12hr fcst	03/12/2020 11Z 11hr fcst	03/12/2020 12Z 10hr fcst
25 100 200 300	25 100 200 300	25 100 200 300

Fig. 42. Time-lagged 1-h maximum updraft helicity (graphic product). Three consecutive HRRRX model forecasts of 1-h max 2-5 km UH are displayed on one image, with each forecast having a separate color. All forecasts are from the 12z/12 March HRRRX and are valid at the same time, 22z/12 March


HRRRX 03/12/2020 (12:00) 24h fcst - Experimental
Run Total 1-6km Max Updraft Helicity (over prev hour) (m²/s²)
Valid 03/13/2020 12:00 UTC

HRRRX 03/12/2020 (12:00) 24h fcst - Experimental   Valid 03/13/2020 12:00 UTC
Run Total 1-6km Min Updraft Helicity (over prev hour) (m²/s²)
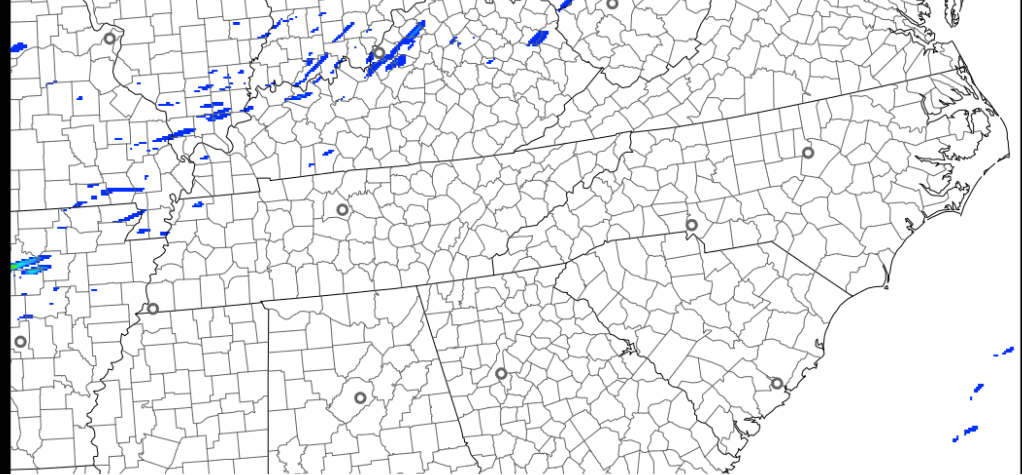
HRRRX 03/12/2020 (12:00) 24h fcst - Experimental   Valid 03/13/2020 12:00 UTC
Run Total 2-5km Max Updraft Helicity (over prev hour) (m²/s²)
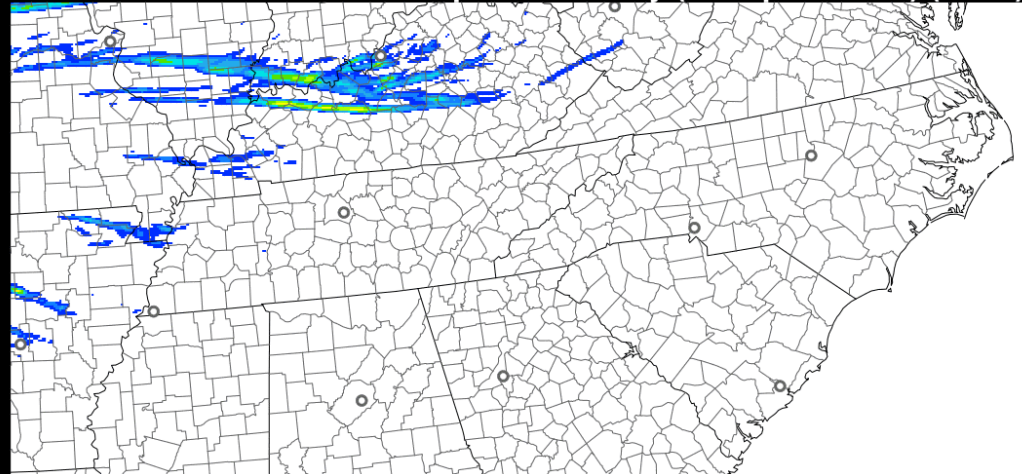
HRRRX 03/12/2020 (12:00) 24h fcst - Experimental   Valid 03/13/2020 12:00 UTC
Run Total 2-5km Min Updraft Helicity (over prev hour) (m²/s²)

43

HRRRX 03/12/2020 (12:00) 24h fcst - Experimental   Valid 03/13/2020 12:00 UTC
Run Total 0-3km Max Updraft Helicity (over prev hour) (m^2/s^2)

HRRRX 03/12/2020 (12:00) 24h fcst - Experimental   Valid 03/13/2020 12:00 UTC
Run Total 0-2km Max Updraft Helicity (over prev hour) (m^2/s^2)

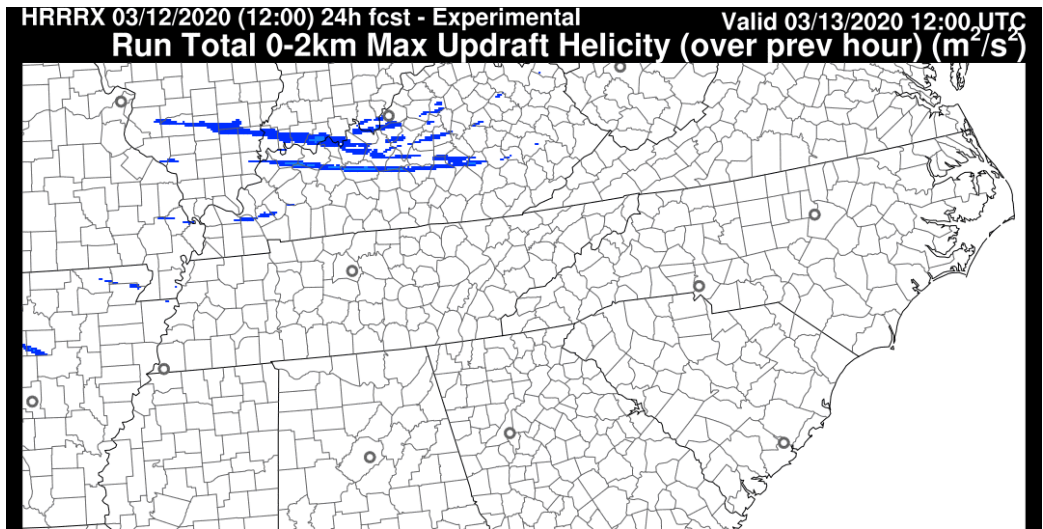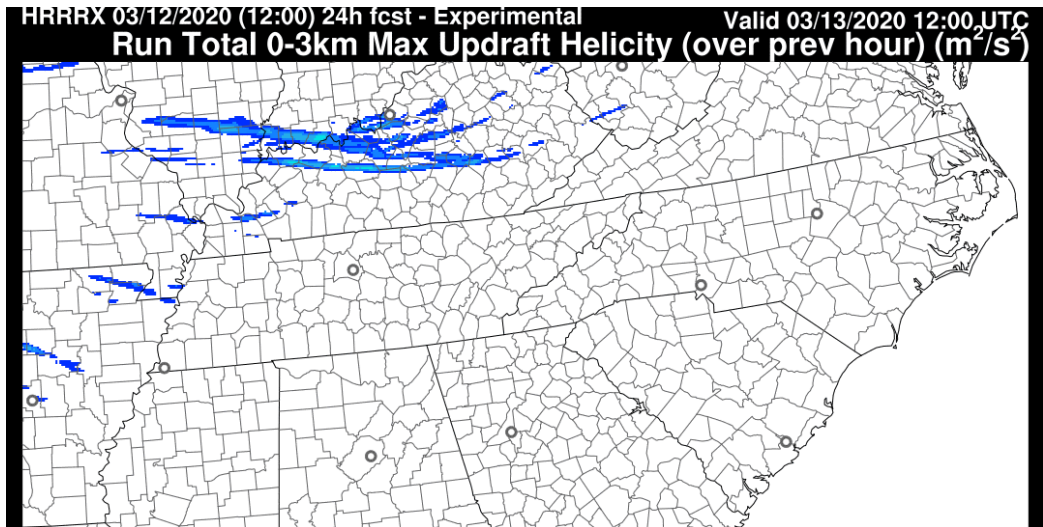25 50 75 100 125 150 175 200 225 250 275 300
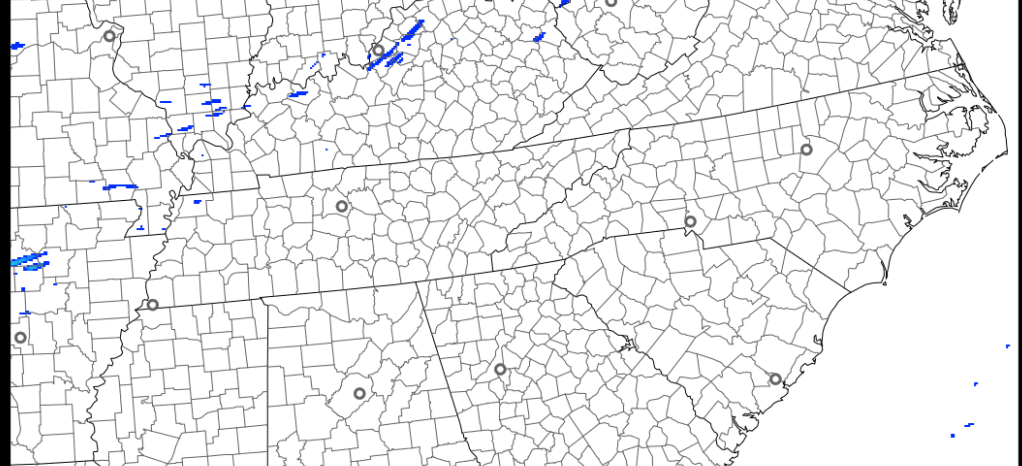
Fig. 43. UH maximum/minimum values. Forecasters have found that it can be easier to view UH values as tracks over a period of time, which can be useful since supercells can last for many hours, both in the model and the real world. On the HRRR webpage, UH tracks are displayed for max and min UH for all the levels that 1-h tracks are also available: 1-6 km, 2-5 km, 0-3 km and 0-2 km AGL. The forecasts shown above are all 24-h UH tracks ending at 12z/13 March for these various levels for both max and min UH values, all from the 12z/12 March HRRRX. There were several supercells on this day producing severe weather including a few tornadoes.

iv. Vertical velocity

Hourly maximum updraft velocity / downdraft velocities are the maximum upward/downward vertical velocities (m s^{-1}) between the surface and 100 hPa (Fig. 44). They do not indicate where in the vertical column the maximum occurred or when during the hour. Hourly mean vertical velocity is the average vertical velocity (m s^{-1}) between sigma level 0.8 and 0.5 (approximately 800 hPa and 470 hPa).
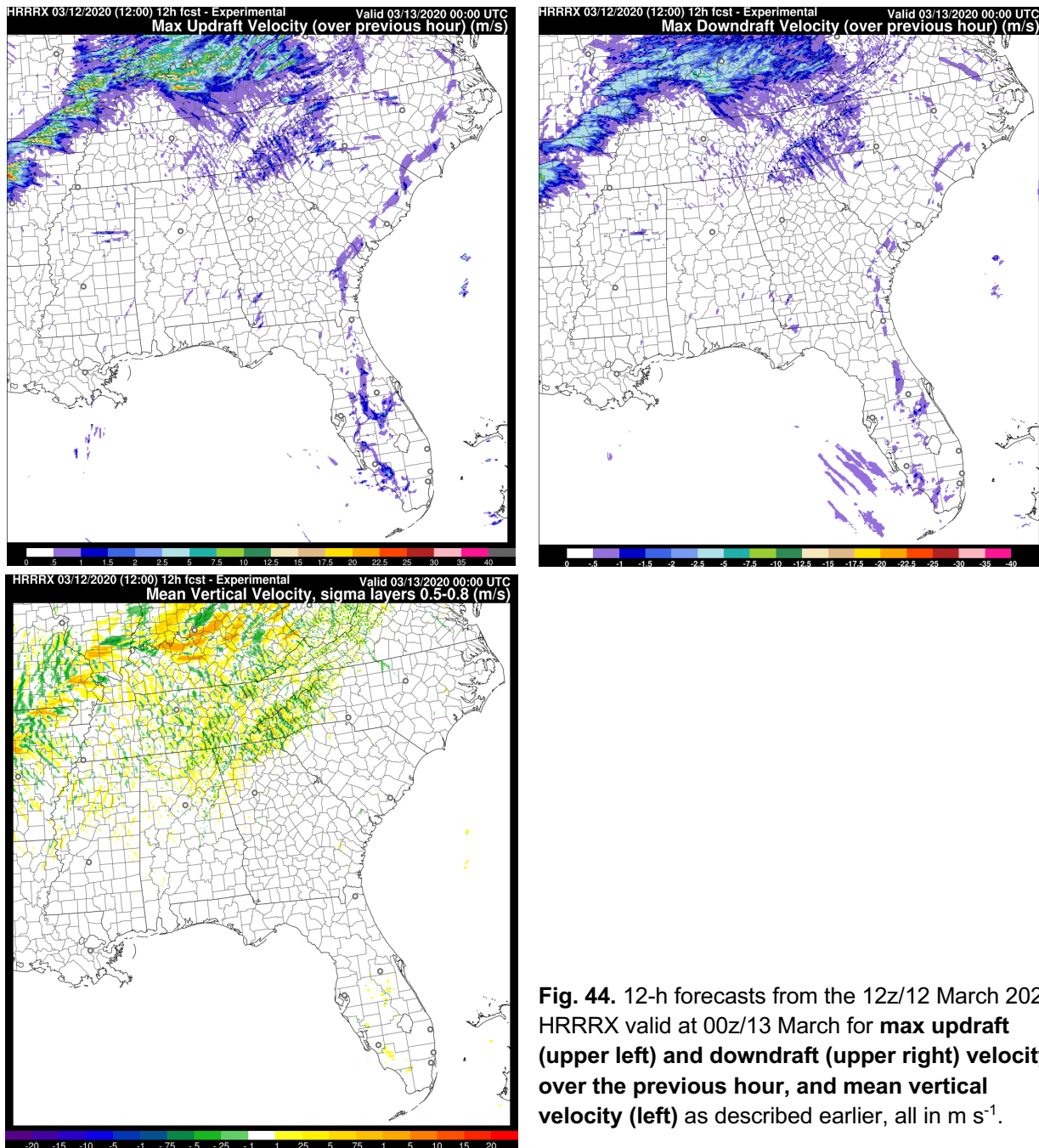

Fig. 44. 12-h forecasts from the 12z/12 March 2020 HRRRX valid at 00z/13 March for **max updraft (upper left) and downdraft (upper right) velocity over the previous hour, and mean vertical velocity (left)** as described earlier, all in m s^{-1}.

v. Vertical vorticity

Vertical vorticity is another diagnostic measuring the strength of low-level rotation within or outside of the convection and does not take into account updraft strength. Hourly maximum vertical vorticity is diagnosed in the HRRR for the 0-1 km layer and the 0-2 km layer (Fig. 45).
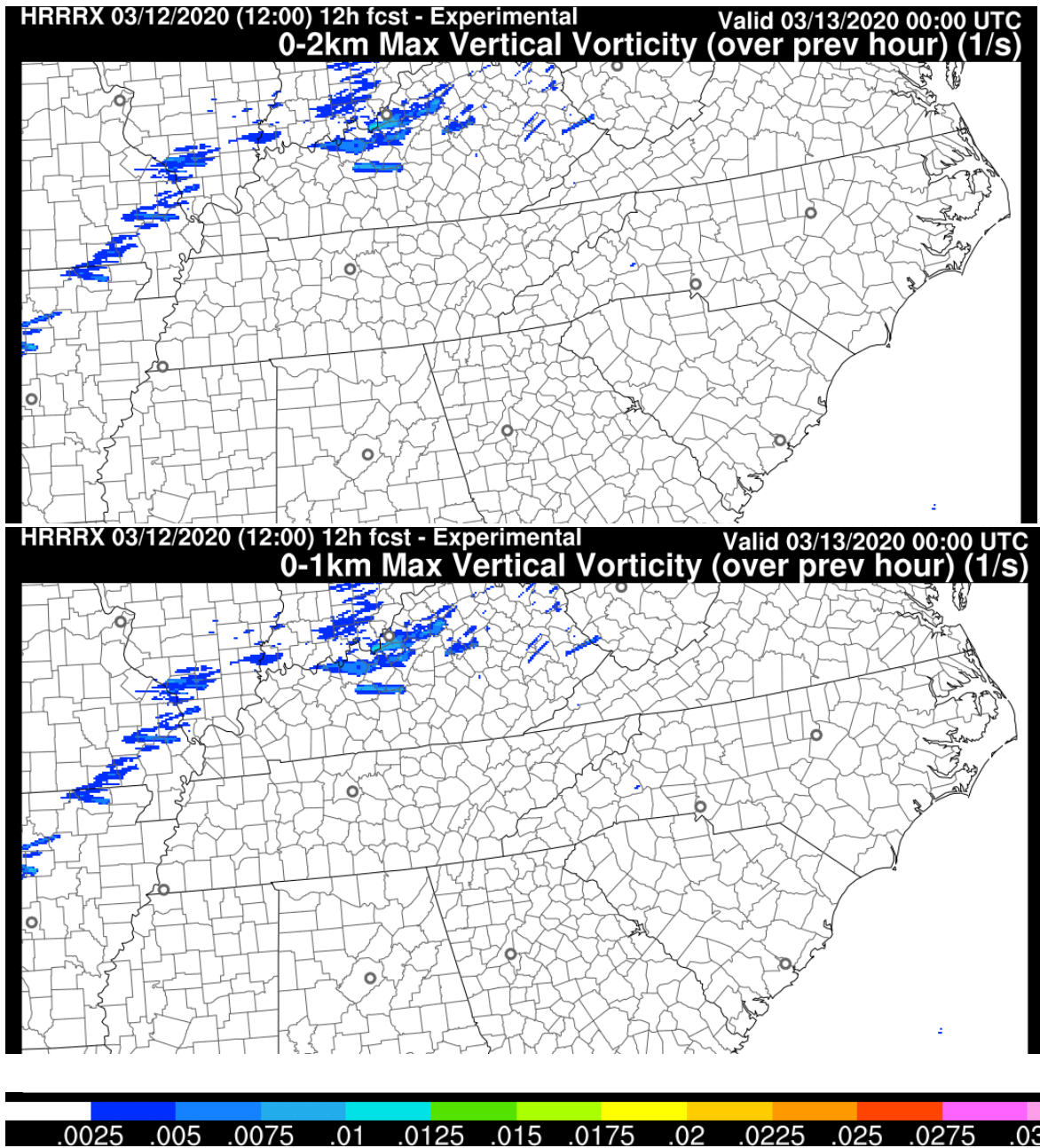

Fig. 45. Vertical vorticity (s^{-1}). For the 0-2 km (AGL) layer (top) and 0-1 km layer (bottom), 12h forecast valid at 00z/13 March from the 12z/12 March HRRRX.

vi. Vertically integrated liquid (VIL)

VIL is calculated from reflectivity to produce an estimate of *vertically integrated liquid* in kg m^{-2}. For an average vertical profile within a convective storm, 12 kg m^{-2} VIL is very roughly equivalent to a 50 dBZ reflectivity although VIL is, by definition a vertically integrated quantity. Two different VIL diagnostics are described below.

VIL (hydrometeor-based diagnostic): Uses a vertical summation of three microphysics hydrometeors including rain, snow, and graupel mixing ratios (no cloud water or cloud ice) in each model column. This diagnostic approach assumes a linear relationship between contributions from different hydrometeors even though the actual relationship is nonlinear.

VIL (radar-based diagnostic): Involves computing model radar reflectivity (*Z*) at all levels in each model column from the precipitation hydrometeors (using both mixing ratios and number concentrations) and then using the familiar mapping of reflectivity factor to VIL (vertical integral of $3.44 * Z^{4/7}$, see Greene and Clark 1972) to produce a field called "Radar VIL." This method is designed to better approximate "observed" VIL from WSR-88D (and other) radars. The radar VIL diagnostic tends to produce lower values when compared to the hydrometeor VIL field, especially around the periphery of more intense moist convective updrafts.
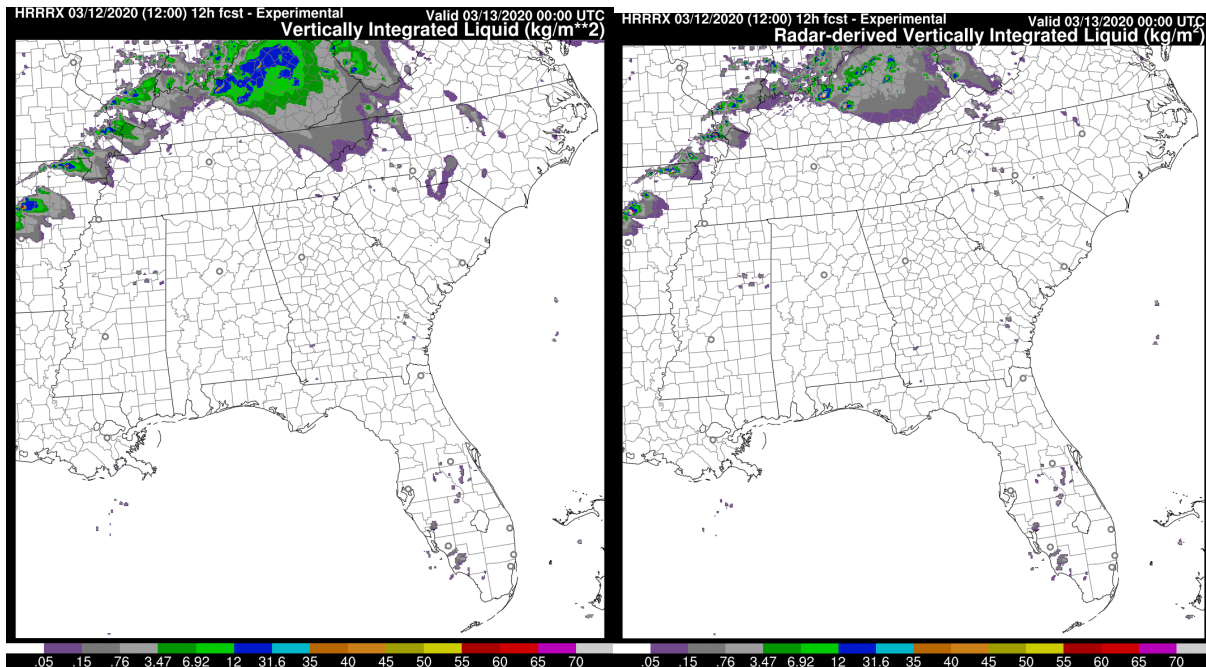

Fig. 46. Vertically integrated liquid. Hydrometeor-based diagnostic (left) and radar-based diagnostic (right). Units - kg m^{-2}. Both are 12-h forecasts valid at 00z/13 March from the 12z/12 March HRRRX.

vii. Echo-top level

Maximum height (in m above sea level) at which reflectivity exceeds 18 dBZ (Fig. 47) in a column. Calculated from vertical profile of reflectivity.
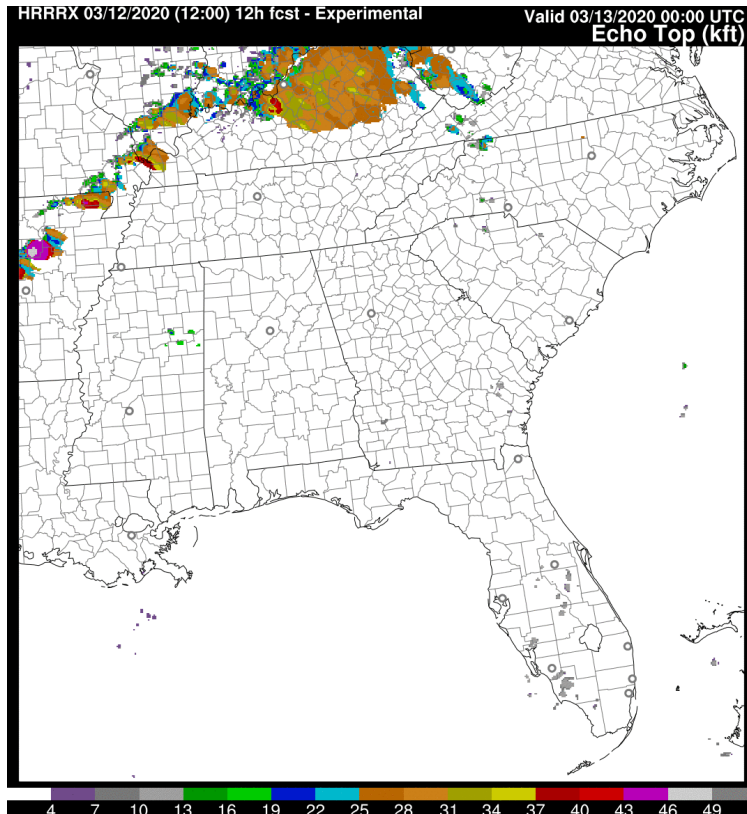

Fig. 47. Echo top. 12-h forecast from the 12z/12 March 2020 HRRRX valid at 00z/13 March. Units shown in graphic - kft ASL.

viii. Hourly maximum/minimum fields

Maximum hourly fields contain the maximum value across every model time-step (20 seconds in HRRR model) at each grid point during that hour. Care must be taken to interpret these fields because one cannot tell when during the hour a feature occurred. Spatial structure could imply one feature moving or multiple features. Hourly maxima can be used to help identify temporal and spatial phase errors in the forecast, and to help infer if features are transient or longer-lived. Hourly maximum fields are provided for the following variables (all of which are described earlier in this section):

- Radar reflectivity at 1 km AGL
- Radar reflectivity at -10°C
- Lightning threat
- Updraft helicity
- Vertical vorticity
- 10-m wind
- Updraft velocity
- Downdraft velocity

I. Other upper-air diagnostics

i. Tropopause pressure

In the RAP, tropopause pressure is diagnosed in the standard Unipost configuration with a surface-upward search for first occurrence of a 3-layer mean lapse rate less than or equal to a critical lapse rate (2 K km^{-1}) in accordance with WMO definition of the tropopause. Low tropopause regions correspond to upper-level waves and give a quasi-3D way to look at upper-level potential vorticity. They also correspond well to dry (warm) areas in water vapor satellite images, since stratospheric air is very dry.

ii. Vertical velocity

Following NCEP Unipost convention, vertical velocity in m/s is converted to omega in Pa/s using the formula omega = -rho*g*w, where rho is air density and g = 9.80665 m s^{-2}.
(The vertical motion is instantaneous (at a given time step) and is not time-averaged.)

Fig. 48. 700 hPa vertical velocity (-Pa s^{-1}). 12h forecast from the 12z/12 March 2020 HRRRX valid at 00z/13 March.

iii. Freezing levels

Two sets of freezing levels are output from RAP/HRRR, one searching in the column from the bottom up, and one searching from the top down. Of course, these two sets may be equivalent under many situations, but they may sometimes identify multiple freezing levels (important for aviation). The bottom-up algorithm will return the surface as the freezing level if any of the bottom 3 native levels (up to about 80 m above the surface) are below freezing (per instructions from the NOAA Aviation Weather Center, which uses this product). The top-down freezing level returns the first level at which the temperature goes above freezing searching from the top downward. For both the top-down and bottom-up algorithms, the freezing level is actually interpolated between native levels to estimate the level at which the temperature goes above or below freezing.

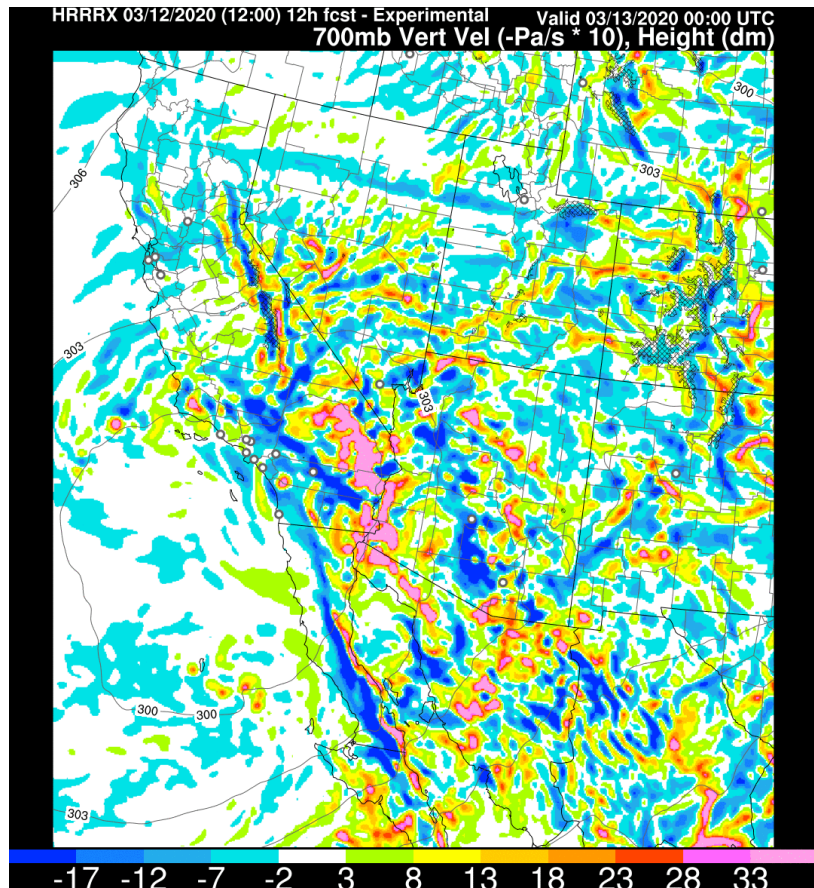iv. Isobaric level vs. native level output for HRRR and RAP

Native-level fields using the model-native levels from HRRR and RAP are never horizontally smoothed. By contrast, isobaric fields are horizontally smoothed for temperature, height, RH, and u/v components of horizontal winds since these fields are often used for horizontal maps. Isobaric fields are output with 25-hPa vertical spacing. Isobaric fields are too smooth to see structure related to orographic effects. For studies of local structure (e.g., orographic, coastal, storm, others), users are advised to use native-level data and not use isobaric data.

J. Smoke-related diagnostics *(introduced with HRRRv4/RAPv5)*

Beginning with the RAPv5 / HRRRv4 which was implemented at NCEP in Dec 2020, both systems (including HRRR-Alaska) explicitly predict concentrations of wildfire smoke at each 3-d grid point. Data assimilation using fire radiative power data from satellites and model effect on radiation from smoke are described by Ahmadov et al (2017). These diagnosed variables below related to smoke are output for RAPv5 and HRRRv4 (CONUS and Alaska).

i. Near-surface smoke

A near-surface smoke diagnostic is provided to downstream users via GRIB2 files, which contain 2D variables. This variable is simply the explicit smoke concentration on the lowest model level (~8 m AGL at sea level). The smoke concentration is in the units of μg m^{-3} (micrograms per cubic meter).
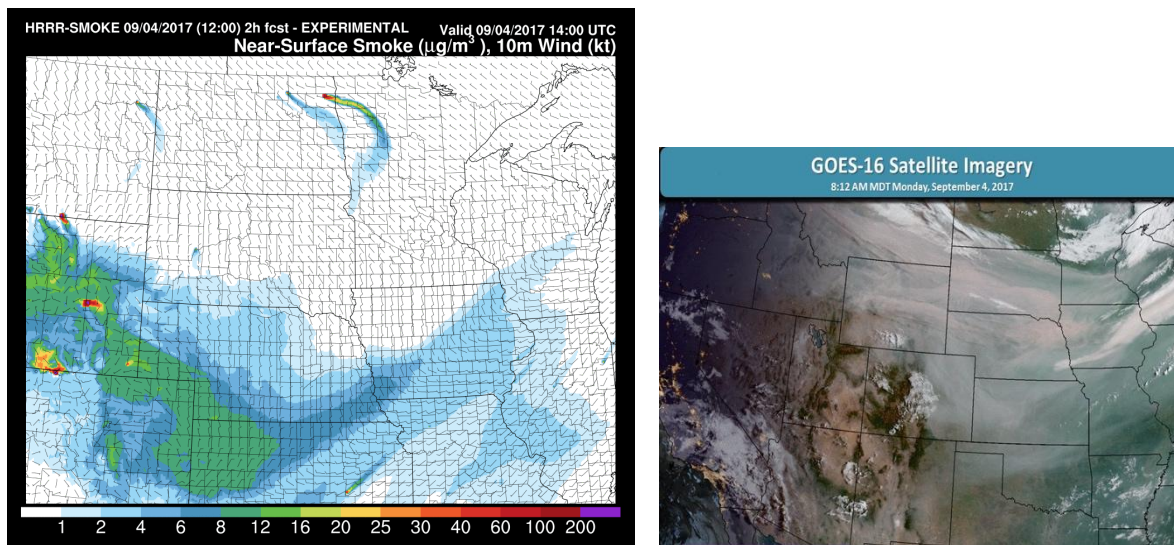

Fig. 49. Near-surface smoke. **(left)** From HRRRX (with 10-m wind) for a case of widespread western U.S. fires on 4 September 2017. **GOES-16 GeoColor imagery (right)** shows the observed extent of smoke in the atmosphere, which is likely more comparable to the HRRR forecast product shown below.

ii. Vertically integrated smoke

In addition to the near-surface smoke, a vertically integrated smoke is diagnosed, in which smoke concentrations are summed across all vertical levels. Units - mg m^{-2}.
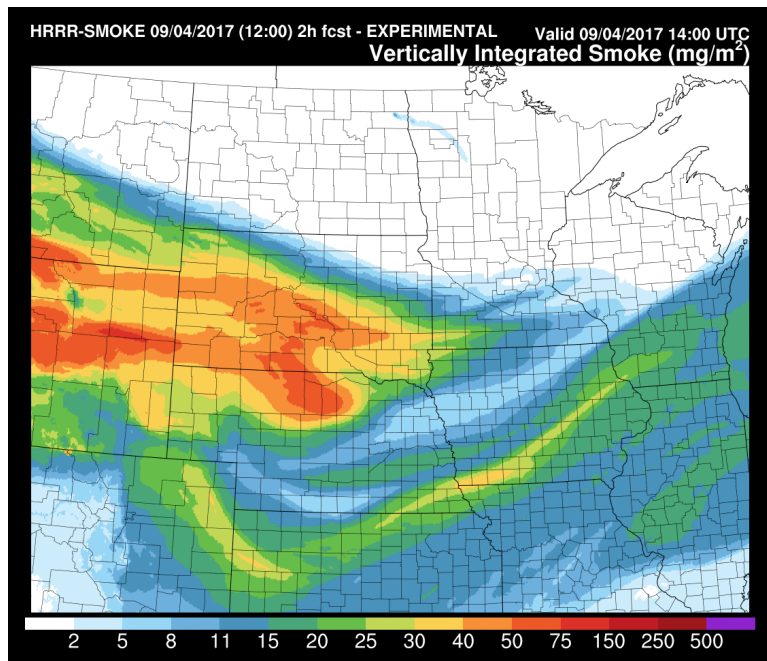

Fig. 50. Vertically integrated smoke. From HRRRX for the same case of widespread western U.S. fires on 4 September 2017.

iii. Aerosol optical depth (not shown)

A 2-D aerosol optical depth (AOD) for smoke is calculated by integrating the smoke extinction across all vertical levels. It should be noted that the AOD (see 'AOTK' variable in the GRIB2 files from RAP/HRRR-Smoke) does not include the contribution of other aerosols (e.g., urban pollution, dust). AOD is a unitless quantity.

3. References

Adams-Selin, R. D., and C. L. Ziegler, 2016: Forecasting hail using a one-dimensional hail growth model within WRF. *Mon. Wea. Rev,* **144,** 4919-4939. https://doi.org/10.1175/MWR-D-16-0027.1

Ahmadov, R., G. Grell, E.P. James, I. Csiszar, M. Tsidulko, R.B. Pierce, S. McKeen, S.G. Benjamin, C.A. Alexander, G. Pereira, S. Freitas, M. Goldberg, 2017: Using VIIRS Fire Radiative Power data to simulate biomass burning emissions, plume rise and smoke transport in a real-time air quality modeling system. IEEE International Geoscience and Remote Sensing Symposium, New York, 2806-2808. https://ieeexplore.ieee.org/document/8127581

Aligo, E.A., B. Ferrier, and J.R. Carley, 2018: Modified NAM microphysics for forecasts of deep convective storms. *Mon. Wea. Rev.*, **146**, 4115-4153.

Benjamin, S. G., and P. A. Miller, 1990: An alternative sea level pressure reduction and a statistical comparison of geostrophic wind estimates with observed surface winds. *Mon. Wea. Rev.,* **118,** 2099-2116. https://doi.org/10.1175/1520-0493(1990)118<2099:AASLPR>2.0.CO;2.

Benjamin, S. G., D. Dévényi, S. S. Weygandt, K. J. Brundage, J. M. Brown, G. A. Grell, D. Kim, B. E. Schwartz, T. G. Smirnova, T. L. Smith, and G. S. Manikin, 2004: An hourly assimilation/forecast cycle: The RUC. *Mon. Wea. Rev.*, **132**, 495-518. https://doi.org/10.1175/1520-0493(2004)132<0495:AHACTR>2.0.CO;2.

Benjamin, S. G., S. S. Weygandt, J. M. Brown, M. Hu, C. R. Alexander, T. G. Smirnova, J. B. Olson, E. P. James, D. C. Dowell, G. A. Grell, H. Lin, S. E. Peckham, T. L. Smith, W. R. Moninger, J. S. Kenyon, and G. S. Manikin, 2016a: A North American hourly assimilation and model forecast cycle: The Rapid Refresh. *Mon. Wea. Rev.,* **144,** 1669-1694. http://dx.doi.org/10.1175/MWRF-D-15-0242.1.

Benjamin, S. G., J. M. Brown, and T. G. Smirnova, 2016b: Explicit precipitation-type diagnosis from a model using mixed-phase bulk cloud-precipitation microphysics parameterization. *Wea. Forecasting,* **31,** 609-619. https://doi.org/10.1175/WAF-D-15-0136.1.

Bunkers, M. J., B. A. Klimowski, J. W. Zeitler, R. L. Thompson, and M. L. Weisman, 2000: Predicting supercell motion using a new hodograph technique. *Wea. Forecasting,* **15,** 61-79. https://doi.org/10.1175/1520-0434(2000)015<0061:PSMUAN>2.0.CO;2.

Dowell, D. C.., C. R. Alexander, E. P. James, S. S. Weygandt, S. G. Benjamin, G. S. Manikin, B. T. Blake, J. M. Brown, J. B. Olson, M. Hu, T. G. Smirnova, T. Ladwig, J. Kenyon, and R. Ahmadov, 2021: The High-Resolution Rapid Refresh (HRRR): An hourly updating convection permitting forecast model. Part I: Motivation and system description. *Mon. Wea. Rev.,* manuscript in preparation.

Greene, D.R. and R.A. Clark, 1972: Vertically integrated liquid water -- A new analysis tool. *Mon. Wea. Rev.,* **100,** 548-552. *https://doi.org/10.1175/1520-0493(1972)100<0548:VILWNA>2.3.CO;2*

Grell, G. A., and D. Dévényi, 2002: A generalized approach to parameterizing convection combining ensemble and data assimilation techniques. *Geophys. Res. Letters,* **29 (14),** 38-1-38-4. https://doi.org/10.1029/2002GL015311.

Grell, G. A. and S. R. Freitas, 2014: A scale and aerosol aware stochastic convective parameterization for weather and air quality modeling. *Atmos. Chem. Phys.,* **14,** 5233-5250. https://doi.org/10.5194/acp-14-5233-2014.

Griffin, S. M., J. A. Otkin, C. M. Rozoff, J. M. Sieglaff, L. M. Cronce, C. R. Alexander, T. L. Jensen, and J. K. Wolff, 2017: Seasonal analysis of cloud objects in the High-Resolution Rapid Refresh (HRRR) model using object-based verification. *J. Appl. Meteor. Climatol.,* **56,** 2317-2334. https://doi.org/10.1175/JAMC-D-17-0004.1.

Han, Y., P. van Delst, Q. Liu, F. Weng, B. Yan, R. Treason, and J. Derber, 2006: JCSDA Community Radiative Transfer Model (CRTM)--Version 1. NOAA Tech. Re. NESDIS 122, 33 pp.

James, E. P., C. R. Alexander, D. C. Dowell, S. S. Weygandt, S. G. Benjamin, G. S. Manikin, J. M. Brown, J. B. Olson, M. Hu, T. G. Smirnova, T., Ladwig, and J. Kenyon, 2021: The High-Resolution Rapid Refresh (HRRR): An hourly updating convection permitting forecast model. Part II: Forecast performance. *Mon. Wea. Rev.,* manuscript in preparation.

Koren, V., J. Schaake, K. Mitchell, Q.-Y. Duan, F. Chen, J. M. Baker, 1999: A parameterization of snowpack and frozen ground intended for NCEP weather and climate models. *J. Geophys. Res.,* **104,** 19569-19585. https://doi.org/10.1029/1999JD900232.

McCaul, E. W., Jr., S. J. Goodman, K. M. LaCasse, and D. J. Cecil, 2009: Forecasting lightning Thread using cloud-resolving model simulations. *Wea. Forecasting,* **24,** 709-729. https://doi.org/10.1175/2008WAF2222152.1.

Olson, J. B., J. S. Kenyon, I. Djalalova, L. Bianco, D. D. Turner, Y. Pichugina, A. Choukulkar, M. D. Toy, J. M. Brown, W. M. Angevine, E. Akish, J.-W. Bao, P. Jimenez, B. Kosovic, K. A. Lundquist, C. Draxl, J. K. Lundquist, J. McCaa, K. McCaffrey, K. Lantz, C. Long, J. Wilczak, R. Banta, M. Marquis, S. Redfern, L. K. Berg, W. Shaw, and J. Cline, 2019a: Improving wind energy forecasting through numerical weather prediction model development. *Bull. Amer. Meteor. Soc.,* **100**, 2201-2220. https://doi.org/10.1175/BAMS-D-18-0040.1.

Olson, J. B., J. S. Kenyon, W. M. Angevine, J. M. Brown, M. Pagowski, and K. Sušelj, 2019b: A description of the MYNN-EDMF scheme and coupling to other components in WRF-ARW. NOAA Tech. Memo. OAR GSD 61, 37 pp., https://doi.org/10.25923/n9wm-be49 .

Otkin, J. A., D. J. Posselt, E. R. Olson, H.-L. Huang, J. E. Davies, J. Li, and C. S. Velden, 2007: Mesoscale numerical weather prediction models used in support of infrared hyper-Spectral measurements simulation and product algorithm development. *J. Atmos.*

Oceanic Technol., **24,** 585-601. https://doi.org/10.1175/JTECH1994.1.

Peckham, S. E., T. G. Smirnova, S. G. Benjamin, J. M. Brown, and J. S. Kenyon, 2016: Implementation of a digital filter initialization in the WRF model and its application in the Rapid Refresh. *Mon. Wea. Rev.,* **144,** 99-106. https://doi.org/10.1175/MWR-D-15-0219.1.

Pondeca, M.S.F.V. de, G.S. Manikin, G. DiMego, S.G. Benjamin, D.F. Parrish, R.J. Purser, W.-S. Wu, J. Horel, Y. Lin, R.M. Aune, D. Keyser, L. Anderson, B. Colman, G. Mann, and J. Vavra, **2011**: The Real-Time Mesoscale Analysis at NOAA's National Centers for Environmental Prediction: Current Status and Development. *Wea. Forecasting*, **26**, 593-612.

Smirnova, T. G., J. M. Brown, S. G. Benjamin, and J. S. Kenyon, 2016: Modifications to the Rapid Update Cycle Land Surface Model (RUC LSM) available in the Weather Research and Forecasting (WRF) model. *Mon. Wea. Rev.,* **144,** 1851-1865. https://doi.org/10.1175/MWR-D-15-0198.1.

Stoelinga, M. T., and T. T. Warner, 1999: Nonhydrostatic, mesobeta-scale model simulations of cloud ceiling and visibility for an east coast winter precipitation event. *J. Appl. Meteor.,* **38,** 385-404. https://doi.org/10.1175/1520-0450(1999)038<0385:NMSMSO>2.0.CO;2.

Thompson, G., P. R. Field, R. M. Rasmussen, and W. D. Hall, 2008: Explicit forecasts of winter precipitation using an improved bulk microphysics scheme. Part II: Implementation of a new snow parameterization. *Mon. Wea. Rev.,* **136,** 5095-5115. https://doi.org/10.1175/2008MWR2387.1.

Thompson, G., and T. Eidhammer, 2014: A study of aerosol impacts on clouds and precipitation development in a large winter cyclone*. J. Atmos. Sci.**, 71**, 3636-3658. https://doi.org/10.1175/JAS-D-13-0305.1.